

MASARYKOVA
UNIVERZITA

PŘÍRODOVĚDECKÁ FAKULTA

**Gravitační vlny: nové okno do
vesmíru**

Bakalářská práce

LEONTÝNA HERGETOVÁ

Brno, jaro 2024

MASARYKOVA
UNIVERZITA

PŘÍRODOVĚDECKÁ FAKULTA

Gravitační vlny: nové okno do vesmíru

Bakalářská práce

LEONTÝNA HERGETOVÁ

Vedoucí práce: Mgr. Ing. arch. Petr Kurfürst, Ph.D.

Ústav teoretické fyziky a astrofyziky

Brno, jaro 2024

MUNI
PŘÍRODOVĚDECKÁ
FAKULTA

Bibliografický záznam

Autor: Leontýna Hergetová
Přírodovědecká fakulta
Masarykova univerzita
Ústav teoretické fyziky a astrofyziky

Název práce: Gravitační vlny: nové okno do vesmíru

Studijní program: Fyzika

Obor: Astrofyzika

Vedoucí práce: Mgr. Ing. arch. Petr Kurfürst, Ph.D.

Akademický rok: 2023/2024

Počet stran: xx + 87

Klíčová slova: Gravitační vlny, Detekce vln, Obecná teorie relativity, Advanced LIGO, Interferometrické detektory, Zpracování signálu, Observatoře gravitačních vln, Splynutí neutronových hvězd, Splynutí dvojité černé díry, Teoretický průběh vln

Bibliographic record

Author: Leontýna Hergetová
Faculty of Science
Masaryk University
Department of Theoretical Physics and Astrophysics

Title of Thesis: Gravitational waves: a new window into space

Degree Programme: Physics

Field of Study: Astrophysics

Supervisor: Mgr. Ing. arch. Petr Kurfürst, Ph.D.

Academic Year: 2023/2024

Number of Pages: xx + 87

Keywords: Gravitational waves, Wave detection, General Theory of Relativity, Advanced LIGO, Interferometric detectors, Signal processing, Gravitational wave observatories, Neutron star mergers, Binary black hole mergers, Theoretical waveform

Abstrakt

V této bakalářské práci se věnujeme studiu gravitačních vln. Cílem je představit problematiku gravitačních vln a následně analyzovat tři z nejzámnějších detekcí gravitačních vln GW150914, GW170814 a GW170817. V teoretické části uvedeme, co jsou to gravitační vlny, jak je měříme a jaký je jejich fyzikální popis. Ve statistické části se pokusíme analyzovat naměřená data zmíněných detekcí, vypočítat teoretickou křivku k takzvané *chirp function* získané úpravou naměřených dat, a sestrojít spektrogramy, kde bude vizuálně znázorněn *chirp*.

Abstract

In this bachelor thesis, we will examine gravitational waves. Our goal is to introduce problems of gravitational waves, following up with an analysis of three of the most known gravitational wave detections, GW150914, GW170814, and GW170817. In the theoretical part, we will explain what gravitational waves are, how to detect them, and their physical background. The statistical part will be devoted to analyzing measured data, calculating theoretical waveform of the so-called *chirp function* that was obtained from measured data, and constructing spectrograms where the *chirp* will be visually displayed.

ZADÁNÍ
BAKALÁŘSKÉ PRÁCE

Akademický rok: 2023/2024

Ústav: Ústav teoretické fyziky a astrofyziky**Studentka:** Leontýna Hergetová**Program:** Fyzika**Specializace:** Astrofyzika

Ředitel ústavu PŘF MU Vám ve smyslu Studijního a zkušebního řádu MU určuje bakalářskou práci s názvem:

Název práce: Gravitační vlny: nové okno do vesmíru**Název práce anglicky:** Gravitational waves: a new window into space**Jazyk závěrečné práce:** angličtina**Oficiální zadání:**

Although the theoretical background predicting gravitational waves has been known for over a hundred years, we can detect them only relatively recently. Several such detectors operate worldwide, collecting datasets from about a hundred events produced by merging stellar-size compact objects. The catastrophic events leading to the detectable gravity wave emissions occur at cosmological distances and are the most energetic processes in the universe. They perform the significant pieces to the puzzle of multimessenger astronomy; in some cases can be identified with a source of electromagnetic radiation which enables their precise localization and observational confirmation of other essential characteristics. In any case, gravity wave astrophysics is a challenging and fastly developing field of modern science.

Literatura:

LOINGER, Angelo. *On black holes and gravitational waves*. Pavia: La Goliardica Pavese. xxii, 129. ISBN 8878303712. 2002.

Vedoucí práce: Mgr. Ing. arch. Petr Kurfürst, Ph.D.**Konzultant:** RNDr. Michal Zajaček, PhD.**Datum zadání práce:** 28. 3. 2023**V Brně dne:** 6. 4. 2024

Zadání bylo schváleno prostřednictvím IS MU.

Leontýna Hergetová, 9. 11. 2023

Mgr. Ing. arch. Petr Kurfürst, Ph.D., 21. 11. 2023

RNDr. Luboš Poláček, 5. 12. 2023

Poděkování

Na prvním místě bych ráda poděkovala svému vedoucímu Mgr. Ing. arch. Petru Kurfürstovi, Ph. D., za jeho ochotu, pohotovost, rady a hlavně nadšení při vedení této práce. Dále bych chtěla poděkovat i svému konzultantovi RNDr. Michalovi Zajačkovi, PhD. za ochotu a pomoc, kde naše síly nestačily. Nakonec bych chtěla poděkovat svým spolužákům, s kterými jsme se vždy podpořili a své rodině a přátelům, kteří mi dobrou energii posílali dálkově.

Prohlášení

Prohlašuji, že jsem svoji bakalářskou práci vypracovala samostatně s využitím informačních zdrojů, které jsou v práci citovány.

Leontýna Hergetová

Contents

Introduction	1
1 Gravitational waves	3
1.1 How to envisage them	3
1.2 Origin of gravitational waves	4
1.3 How we detect gravitational waves	6
1.3.1 History	6
1.3.2 Brief introduction to the interferometry used in GW detectors	7
1.3.3 Detectors of gravitational waves	10
2 General Theory of Relativity	15
2.1 The origin of GTR	15
2.2 Mathematical form and characterization of EFE	15
2.2.1 Einstein's tensor	16
2.2.2 Ricci curvature tensor	16
2.2.3 Ricci scalar	17
2.2.4 Cosmological constant	18
2.2.5 Constants	18
2.2.6 Energy-momentum tensor	19
3 Answering the question about analysis	21
3.1 Why are we doing the analysis?	21
3.2 How to analyze GWs data	22
3.2.1 Where we got the means used for analysis?	22
3.2.2 Where to obtain data?	30
3.2.3 What else is needed for calculations?	30
4 Analysis and calculation of theoretical waveform	33
4.1 GW150914	33
4.1.1 Measured data	33
4.1.2 Theoretical waveform	36
4.1.3 Spectrograms	40
4.2 GW170814	43
4.2.1 Measured data	43

4.2.2	Theoretical wavefunction	46
4.2.3	Spectrograms	49
4.3	GW170817	52
4.3.1	Measured data	52
4.3.2	Theoretical wavefunction	55
4.3.3	Spectrograms	55
5	Conclusions	59
	References	61
	Index	65
A	Appendix	67
A.1	Codes with steps for GW150914	67
A.1.1	Packages	67
A.1.2	Measured data	67
A.1.3	Theoretical waveform	70
A.1.4	Combination of MD and TW	72
A.1.5	Spectrograms	72
A.2	Code for GW170814	75
A.3	Code for GW170817	82

List of table

3.1	Overview of used constants and conversions.	31
3.2	Used parameters of mergers GW150914, GW170814, and GW170817.	31

List of figures

1.1	Visualization of the gravitational waves and the density changes of two orbiting neutron stars. Credit: STAG Research Centre/Peter Hammond (University of Southampton).	4
1.2	The original scheme of Michelson interferometer. Credit: [8]	9
4.1	Raw Advanced LIGO strain data near GW150914.	34
4.2	ASDs of Advanced LIGO data near GW150914.	35
4.3	Whitened Advanced LIGO strain data near GW150914.	36
4.4	Comparing TW to the MD of GW150914 while changing the parameters from table 3.2: a) values without uncertainties, b) values while adding uncertainties, c) adding uncertainty only in luminosity distance, d) adding uncertainties to both masses.	38
4.5	Comparing TW to the MD of GW150914 while changing the parameters from table 3.2: e) values while subtracting uncertainties, f) subtracting uncertainty only in luminosity distance, g) subtracting uncertainties to both masses, h) subtracting uncertainties from themselves ($D = 440 - 20$ Mpc, $m_1 = 35.6 + 1.6 M_\odot$, $m_2 = 30.6 - 1.4 M_\odot$).	39
4.6	Final TW showcased on whitened strain data near GW150914.	40
4.7	Time-frequency spectrogram of aLIGO H1 raw strain data near GW150914. The sense of the colorbar is explained at the start of the section 4.1.3.	41
4.8	Time-frequency spectrogram of aLIGO L1 raw strain data near GW150914.	42
4.9	Time-frequency spectrogram of aLIGO H1 whitened strain data near GW150914.	42
4.10	Time-frequency spectrogram of aLIGO L1 whitened strain data near GW150914.	43
4.11	Raw Advanced LIGO strain data near GW170814.	44
4.12	ASDs of Advanced LIGO data near GW170814.	45
4.13	Whitened Advanced LIGO strain data near GW170814.	46

4.14	Comparing TW to the MD of GW170814 while changing the parameters from table 3.2: a) values without uncertainties, b) values while adding uncertainties, c) adding uncertainty only in luminosity distance, d) adding uncertainties to both masses.	47
4.15	Comparing TW to the MD of GW170814 while changing the parameters from table 3.2: e) values while subtracting uncertainties, f) subtracting uncertainty only in luminosity distance, g) subtracting uncertainties to both masses, h) subtracting uncertainties from themselves ($D = 600 - 70 \text{ Mpc}$, $m_1 = 30.6 + 2.6 M_\odot$, $m_2 = 25.2 - 1.2 M_\odot$).	48
4.16	Final TW showcased on whitened strain data near GW170814.	49
4.17	Time-frequency spectrogram of aLIGO H1 raw strain data near GW170814.	50
4.18	Time-frequency spectrogram of aLIGO L1 raw strain data near GW170814.	50
4.19	Time-frequency spectrogram of aLIGO H1 whitened strain data near GW170814.	51
4.20	Time-frequency spectrogram of aLIGO L1 whitened strain data near GW170814.	51
4.21	Raw Advanced LIGO strain data near GW170817.	53
4.22	ASDs of Advanced LIGO data near GW170817.	53
4.23	Whitened Advanced LIGO strain data near GW170817.	54
4.24	Final TW showcased on whitened strain data near GW170817.	55
4.25	Time-frequency spectrogram of aLIGO H1 raw strain data near GW170817.	56
4.26	Time-frequency spectrogram of aLIGO L1 raw strain data near GW170817.	56
4.27	Time-frequency spectrogram of aLIGO H1 whitened strain data near GW170817.	57
4.28	Time-frequency spectrogram of aLIGO L1 whitened strain data near GW170817.	57

Introduction

Waves as a phenomenon are a ubiquitous occurrence in physics. Usually, we can observe them as something that oscillators of some kind can cause, for example, waves on a water surface (mechanical waves), music (acoustic waves), or light (electromagnetic radiation), and we can measure the energy that they contain. In most cases, we can understand waves quite easily because we can actually see, perceive, or sense them (usually mechanical or acoustic waves). With light, it is more difficult to understand because of its dual nature (it can be perceived as a particle and as a wave). We can also perceive the energy they hold by, for example, feeling the waves hitting us while swimming in the sea.

Another well-known phenomenon is gravity. It was explained by Isaac Newton in the 17th century in his work "De motu corporum in gyrum," where he established it as a centripetal force [1]. In Newtonian physics, we can say it is interaction based on the 3rd Newton's Law where actions (in this case gravitational interaction) of two objects upon each other are of the same intensity but directed in the opposite direction.

In 1915, Albert Einstein combined these two phenomena in his work about the General Theory of Relativity. He derived an idea that Gravity can be perceived as something generated by the curvature of spacetime that was produced by embedded mass [2]. If such spacetime curvature experiences periodic disturbing, the transversal waves propagate through it, called gravitational waves.

Now it is our job to study, acknowledge, and appreciate their nature.

1 Gravitational waves

This is the start of the theoretical part of this thesis:

The goal is to introduce all the ways how we can perceive gravitational waves (from now GWs). We will start with the basics of how they look in spacetime, their origin, following up with "catching" them and their appearance after detection, and finally how they look after physical formula description.

1.1 How to envisage them

GWs are, as already said, ripples in spacetime. To visualize it, let's say we have a massive bed sheet, preferably without elastics around the perimeter. If we stretch it really tight and fix it only in the corners, we will get a horizontally stretched surface; this is our spacetime.

Now, we can put something on it, for example, an orange ball. For us, this will represent some object in space (it is round and heavy compared to our "spacetime"). After putting our "astronomical object" in the corner of our "spacetime" it will move straight to the center of the bed sheet and a downswing in the middle of the bed sheet will appear. This is how gravity makes ripples in spacetime.

Now, that we know what the interaction between an object and spacetime looks like, we can visualize it as the gravitational interaction of two objects. With our orange ball in the center, we will now use a pink ball, firstly moving parallel to the one side of the bed sheet. The pink ball would trace a spiral while moving closer to the orange one. If both orange and pink balls were moving, we would see ripples similar to this visualization of actual gravitational waves in figure 1.1.

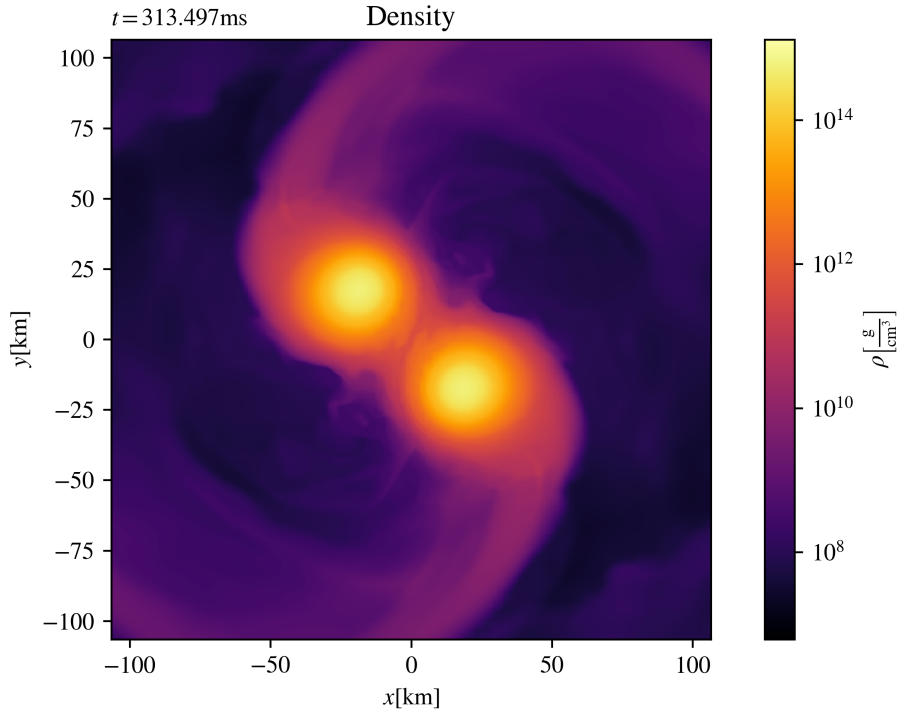


Fig. 1.1: Visualization of the gravitational waves and the density changes of two orbiting neutron stars. Credit: STAG Research Centre/Peter Hammond (University of Southampton).

1.2 Origin of gravitational waves

As a starting point, we need to mention that every physical object that accelerates or is accelerating causes ripples in spacetime and therefore produces GWs, but we need sizable ripples to detect them, ergo we will talk about colossal events.

Detectable GWs are formed by some of the most arduous and powerful processes in the Universe. The most important sources are cataclysmic events such as two objects colliding; for example, black holes, neutron stars, etc. In addition to the collision, the orbital movement before may also be a source of GWs; we can also consider orbiting

without collision, namely in the case of rapidly spinning objects like neutron stars that are imperfect spheres. [3].

Astronomers later defined four categories of GWs to distinguish them and specify which systems or objects generate them. The four categories are:

- Compact Binary Inspiral GWs,
- Continuous GWs,
- Stochastic GWs,
- Burst GWs.

Now, let us describe the classification:

Compact Binary Inspiral GWs are produced by enormous objects orbiting each other. This type of GWs has subtypes based on which objects are the binary members.

We could have *BNS* (*Binary Neutron Stars*) that are two neutron stars orbiting each other, *BBH* (*Binary Black Holes*) that are two black holes orbiting each other, and lastly *NSBH* (*Neutron Star-Black Hole Binary*) that is pair of a neutron star and a black hole.

Each variant has its unique pattern of GWs that depends on the parameters of the pair (how heavy each object is, how the orbit is directed towards the Earth, how far away from each other they are, etc.). However, the main principle of making the GWs is still the same and its called *inspiral* (as we could see in Figure 1.1). [4]

Continuous GWs are expected to be produced by one massive spinning object. A good example could be a non-perfectly spherical neutron star. All the shape imperfections will generate GWs as the neutron star spins. As the name indicates, the GWs do not change frequency and/or amplitude in this case. [4]

Stochastic GWs are interfering GWs. Detecting a signal from two sources would get us a "stochastic signal" which means, detecting a very random pattern (not necessarily unanalyzable but surely unpredictable).

These GWs are very difficult to detect because it is improbable that two strong enough signals would interfere. We can recognize this just by looking at the number of significant sources of continuous or compact binary GWs. Another thing is that there is a faint continuous stochastic signal where we think part of it could be relic GWs from the Big Bang. By detecting it, we would be able to see farther back into the Universe's history. [4]

Burst GWs, as the name indicates, come from unexpected short-periodic sources. These signals are difficult to detect because, as we all know, to be prepared for something unanticipated is almost impossible. [4]

1.3 How we detect gravitational waves

1.3.1 History

Joseph Weber was the first person who tried to detect GWs in the 60s of the 20th century, following the conclusions of the General Theory of Relativity (GTR for short). He constructed 2-meter-long and 1-meter-wide aluminum cylinders with resonance frequency 1660Hz that could measure with 10^{-16} relative accuracy and wrote an article about his discovery in 1969 [5]. His colleagues were sceptical about his detections, which he allegedly did. Others also tried to build similar detectors but no detections were achieved; one of them was Heinz Billing in the early 1970s at the Max Planck Institute [6]. The lack of success is because the detectors were tuned to a single frequency which, as we know today, is not met in GWs whose frequency rapidly changes.

The first indirect detection of GWs was published in a scientific paper by R. A. Hulse and J. H. Taylor in July 1974 in the *Astrophysical Journal*. Hulse and Taylor measured binary pulsar PSR B1913+16 with

a decreasing orbital period, which agreed with GTR, and explained it as a loss of energy emitted in the form of GWs [7].

Later, the GW society started using laser interferometry as the more promising and advanced way of detecting GWs. The early prototypes were built in the 70s of the 20th century. Currently, we have many detectors based on laser interferometry. Now, we will introduce these detectors and the principles they work on.

1.3.2 Brief introduction to the interferometry used in GW detectors

Basics of interference

As it is known, wave interference is a basic term describing the addition or subtraction of wave amplitudes. There are two options for how waves can interfere:

1. Constructively,
2. Destructively.

Constructive interference increases the wave amplitude. We can easily write the resulting wave amplitude of constructive interference W as a sum of the amplitudes of two waves interfering $W_{1,2}$,

$$W_1 + W_2 = W. \quad (1.1)$$

The difference of phases $\Delta\varphi$ of the initial waves needs to be an even multiple of π (applies for phase differences $\Delta\varphi = \dots, -2\pi, 0, 2\pi, \dots$) for the interference to be fully constructive.

Destructive interference is the complete opposite of constructive interference, meaning the final product of the interference is zero. Or, if we say it in a different lingo, the interference of the waves will create a wave with an amplitude equal to zero. With this knowledge, we can write the sum as

$$W_1 + W_2 = 0. \quad (1.2)$$

For the destructive interference the difference of phases $\Delta\varphi$ of the initial waves needs to be on the other hand an odd multiple of π (applies for phase $\Delta\varphi = \dots, -3\pi, -\pi, \pi, 3\pi, \dots$).

The waves have to be coherent (of the same type) for the interference to work. The waves can be of any type if they meet this requirement (ex.: mass, acoustic, surface, etc.). In our case, we will use electromagnetic waves in the form of a laser that can accurately measure the relative amplitude (strain) and phase of GWs. The usage of the laser also meets the other two requirements which are a) the light we are using needs to be monochromatic and b) the light cannot have a random phase.

Michelson interferometer

As we introduced the technique of interferometry, now it is time to introduce the tool of interferometry used in the vast majority of the detectors of GWs, which is based on principles of the Michelson interferometer.

The Michelson interferometer was first introduced in the American Journal Of Science in an article "On the Relative Motion of the Earth and the Luminiferous Ether" [8], where also the original scheme came from (as seen in figure 1.2). If we use labeling from the picture and the original comment from the article for the part labeled 1. in figure 1.2, the Michelson interferometer can be described as

- sa* ... a beam of light,
- ab* ... partly reflected beam of light,
- ac* ... partly transmitted beam of light,
- b,c* ... mirrors returning beams.

With this knowledge, we can figure out how the interferometer works.

At this moment, we know that *a* is some kind of beam splitter that splits the beam of light into two parts perpendicular to each other. From the mirror *b* is returning the partly reflected beam along *ba* and from the mirror *c* the partly transmitted beam along *ca*. After returning to the beam splitter (via the same logic with which the beam was split), the partly reflected beam *ba* will become the partly transmitted beam along *ad* and vice versa with the beam *ca*. After all, if the paths *ab* and *ac* are of equal length, the two beams will interfere along *ad*.

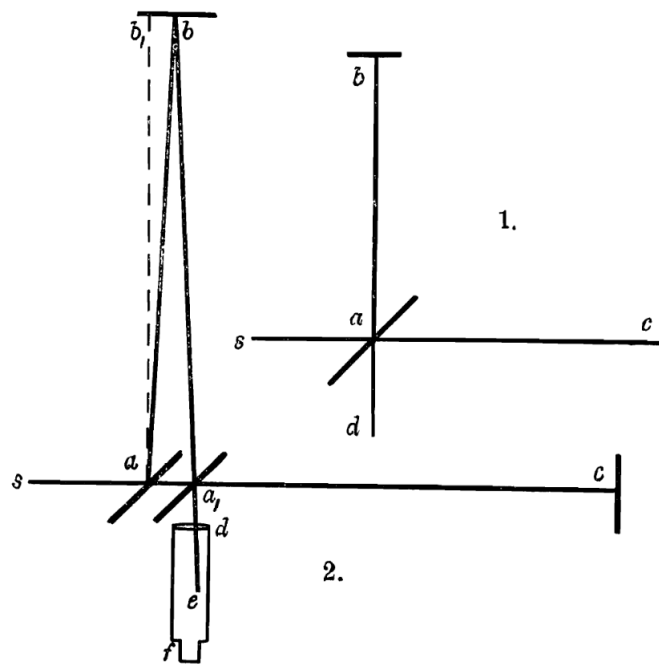


Figure 1.2: The original scheme of Michelson interferometer. Credit: [8]

Application

Now, that we know the technique and tool of interferometry, we need to apply all this to measuring GWs, which is in essence quite understandable after our description. We know that if the beams are equal and go through same-distance routes (which also implies that the "arms" of the interferometer need to be of the same length), they interfere destructively because they are in a counterphase. Now, let us imagine some GWs passing through our interferometer. The laser beams will interact with the GWs (because they are both of a wave character) and the beams will measure different shortening and lengthening of detector arms while going through the two perpendicular "arms" and back. Thanks to that, the beams will interfere constructively or destructively, and we can detect GWs.

1.3.3 Detectors of gravitational waves

GEO600

GEO600, built in 1995, is a GW detector located near Hannover, Germany, operated by the Max Planck Institute for Astrophysics in company with partners from the United Kingdom. This ground-based interferometric (extracting information from interferometry of GWs) detector with 600 meters of arm's length is part of a worldwide network of GW detectors. This network also contains detectors LIGO, Virgo, and KAGRA (we will talk about these detectors within their subsection).[9]

Scientists from GEO600 collaborate with LIGO within the LIGO Scientific Collaboration (LSC), where they focus on directly detecting GWs for further exploration of fundamental physics [10]. They also tightly cooperate with Laser Zentrum Hannover (LZH - independent non-profit institute, where they research and develop laser technology [11]) to help build lasers for Advanced LIGO (aLIGO - an extension of the "initial LIGO" used for the improvement of capabilities of the detectors).

LIGO

Laser Interferometer Gravitational-Wave Observatory (LIGO for short), built from 1994 to 2002 is a national facility for GW research located in the United States. It consists of two multi-kilometer-scale GW detectors, one based in Hanford, Washington, and the other in Livingston, Louisiana. They operate in unison to detect then GWs together.

LIGO is, as mentioned, also one of the detectors of a worldwide GW-detecting network. We also mentioned aLIGO (Advanced LIGO) and "initial LIGO". These are models of LIGO built through the years. The initial LIGO is the original LIGO instrument engaged in science observations from 2002 to 2010. From the end of the Initial LIGO project until 2014, both LIGO detectors were rebuilt to join another project called aLIGO which, as said, improved detectors by enhancing their sensitivity. To this day, engineers from LIGO try to make it more and more sensitive to detect more signals.[12]

LIGO is also planning a sister detector in India (we still do not know where exactly) named very suitably LIGO-India . The detec-

tor would become part of the worldwide network and a member of a collaborative project between the LIGO laboratory in the USA and a consortium of Indian research institutions. The LIGO-India project was approved in 2016 and since then it has been actively worked on by both India and USA. [13]

The LIGO detector made its first official detection of GWs after installing aLIGO named GW150914 together with Virgo as LSC (LIGO Scientific Collaboration) and Virgo Collaboration which we will analyze in the statistical part of this thesis. [14]

Virgo

Virgo, built from 1997 to 2003 (when it was inaugurated) is an interferometric detector located in the countryside near Pisa, Italy. Before the year 2000, the building of Virgo was supervised by the Italian Institute for Nuclear Physics INFN (*Istituto Nazionale di Fisica Nucleare*) and the French National Centre for Scientific Research CNRS (*Centre National de la Recherche Scientifique*). These two institutes were the ones that approved the proposal to build Virgo and in the year 2000, they established the European Gravitational Observatory (EGO for short). EGO was primarily created to take care of maintaining and operating the Virgo detector, now it is also in the management of the infrastructure of the site, the computing center, and the promotion of a variety of R&D (research and development) activities.

Later came an upgrade of Virgo called Advanced Virgo. This project aimed to improve detection capabilities similar to aLIGO in 2014. It was completed in 2017 and was ready to join LIGO for the second observation period. During this period, the LVC (LIGO Virgo Collaboration) detected GW170817 which was accompanied by an electromagnetic glint observed both from the Earth and space [15] [16]. Three days before the LVC detected GW170814 by all detectors, the first time that all detectors had picked up any part of a GW. Similar to GW150914, these events were remarkable hence we will include them in the statistical part of this thesis as well.

KAGRA

Kamioka Gravitational Wave Detector (KAGRA for short) also known as Large Scale Cryogenic Gravitational Wave Telescope (LCGT), built from 2010 to 2019 is an underground cryogenic detector managed by the Institute for Cosmic Ray Research (ICRR) of the University of Tokyo located in Kamioka mines, which is in the city of Hida in Gifu, Japan.

As previously mentioned, KAGRA being an underground interferometer allows for improved noise reduction. Situated underground, we can better isolate it from seismic noise and keep the interferometer's mirrors cold enough to reduce thermal noise, thus making the detector detect a wider range of frequencies. [17]

The KAGRA is quite the new detector which means, it was not running during the first (O1) and second observation (O2) run with its "colleagues" LIGO and later Virgo. KAGRA joined them at the end of the third observation run (O3) in the first half of 2020 and since May 2023 they will all work together on observation run four (O4). [18]

Einstein Telescope

The Einstein Telescope (ET) is yet to be built, a European underground third-generation GW detector that would be used for further observations of mergers (especially black hole mergers). Its location is not yet decided but the candidates for its placement are Sardinia, Netherlands, or Germany [19]. Its planned construction beginning is around 2026 and the goal is to start observations in 2035. [20]

LISA

Laser Interferometer Space Antenna (LISA for short) is an anticipated space project from NASA (National Aeronautics and Space Administration) and since 2024 from ESA (European Space Agency). [21]

LISA will be a space interferometer composed of three spacecraft in a triangular formation (with side lengths in millions of kilometers). It will orbit the Sun in a path similar to Earth's orbit, but about a hundred times farther from Earth than the distance to the Moon. Being in space means it will not have to deal with seismic noise. [22]

It will work on the time delay interferometry principle which is different from the ground interferometers we discussed till this point. Time delay interferometry adds time dependence to the interferometry. The basis is the same as in an Earth interferometer (as we explained in subsection 1.3.2) but because the sides of the triangle will be of different lengths (as it is in space-based detectors), the laser light will arrive to the photodetectors at different times which means we need to add the time delay for it to detect "nothing" (so that the laser beams interfere in counterphase and thus cancel each other out). [23]

Thanks to LISA, we would be able to observe and detect distant systems like EMRIs (Extreme Mass Ratio Inspirals - smaller stellar mass black holes).

2 General Theory of Relativity

In this chapter, we will introduce the theory used to understand gravitation in problems of GWs.

We will go through the history of creation, refusal, and final acceptance of the theory as well as its wording with an explanation of mathematical principles used in the resulting and generally accepted formulation.

2.1 The origin of GTR

In 1905, Albert Einstein (from now on only AE) published, among others, 4 papers in which he explained the photoelectric effect, Brownian motion, etc., and especially the paper introducing the special theory of relativity (from now on only STR) where he states that speed of light is finite and sets it as a constant, now having the value $c = 299792458 \text{ m s}^{-2}$.

Later, he realized that STR did not include accelerating objects and was missing an explanation of gravity. So AE, with mathematical help from his dear friend Marcel Grossmann, tried to solve these problems and shed light on these two omitted factors [24]. In 1915 AE published a paper on GTR where he presented the field equations, now known as Einstein field equations (for short EFE) , defined as

$$R_{\mu\nu} - \frac{1}{2}R g_{\mu\nu} + \Lambda g_{\mu\nu} = \frac{8\pi G}{c^4} T_{\mu\nu}. \quad (2.1)$$

2.2 Mathematical form and characterization of EFE

In this section, we will discuss the equation (2.1) for clarity. We will start from the left and continue to the right. Our main source for explanation will be the book *General Relativity - An Introduction for Physicists* [25].

2.2.1 Einstein's tensor

Einstein's tensor contains the first and the second terms in EFE. It is a formal simplification, so we don't need to write the full equation when we don't need to. The definition can be denoted by equation (2.2)

$$G_{\mu\nu} = R_{\mu\nu} - \frac{1}{2}R g_{\mu\nu}. \quad (2.2)$$

The particular terms in the equation are $g_{\mu\nu}$ which is a metric tensor, $R_{\mu\nu}$ which is a Ricci curvature tensor and R which is a Ricci scalar. The Ricci components are explained in subsections 2.2.2 and 2.2.3.

To explain the metric tensor $g_{\mu\nu}$, we first need to say that GW formalism is difficult to build because of its nonlinearity. We need to consider that ripples in spacetime are very weak because we are far away from the source. After considering all this, we can linearize the gravitational field. We will work with just slight deformation of Minkowski flat spacetime defined by tensor (2.3) with a small deviation $h_{\mu\nu}$.

$$\eta_{\mu\nu} = \begin{pmatrix} 1 & 0 & 0 & 0 \\ 0 & -1 & 0 & 0 \\ 0 & 0 & -1 & 0 \\ 0 & 0 & 0 & -1 \end{pmatrix}. \quad (2.3)$$

With this in mind, we can describe our linearized metric tensor for small spacetime perturbations as

$$g_{\mu\nu} \simeq \eta_{\mu\nu} + h_{\mu\nu} + \mathcal{O}(h_{\mu\nu})^2, \quad |h_{\mu\nu}| \ll 1. \quad (2.4)$$

2.2.2 Ricci curvature tensor

Tensor $R_{\mu\nu}$ is the curvature tensor representing how volume in the curved space differs from volume in an Euclidean space [26]. To remind us what an Euclidean space is, it is a space where parallel lines do not cross/cross in infinity, and the sum of angles in a triangle (on a flat surface) is 180° .

The Ricci tensor can be written in matrix representation as a 4×4 symmetric matrix, as seen in (2.5). The tensor $R_{\mu\nu}$ has 2 indices, μ and ν . These indices define different matrix components and they take

the values $\mu, \nu = 0, 1, 2, 3$,

$$R_{\mu\nu} = \begin{pmatrix} R_{00} & R_{01} & R_{02} & R_{03} \\ R_{10} & R_{11} & R_{12} & R_{13} \\ R_{20} & R_{21} & R_{22} & R_{23} \\ R_{30} & R_{31} & R_{32} & R_{33} \end{pmatrix}. \quad (2.5)$$

We can also write Ricci curvature tensor in term of Christoffel symbols,

$$R_{ij} = \partial_k \Gamma_{ij}^k - \partial_j \Gamma_{ik}^k + \Gamma_{ij}^k \Gamma_{km}^m - \Gamma_{im}^k \Gamma_{jk}^m, \quad (2.6)$$

where Γ_{ij}^k is called the Christoffel symbol, written in Einstein's notation. We can apprehend i, j , and k the same as μ and ν , which we already explained. The following relation defines the general form of Christoffel symbols,

$$\Gamma_{ij}^k = \frac{1}{2} g^{km} (\partial_j g_{mi} + \partial_i g_{mj} - \partial_m g_{ij}), \quad (2.7)$$

where g^{km} with any of the aforesaid indexes is a metric tensor.

Ricci tensor, besides a general mathematical/geometrical definition, has also a particular meaning in EFE. It describes changes in the space-time volume that was disturbed by gravitational waves. To explain it more illustratively, it quantifies the volume between two geodesics (the shortest possible line between two points or two events in space-time in given metrics) that were parallel in the first place but now, because of spacetime curvature caused by GWs, they are not. [26]

2.2.3 Ricci scalar

Ricci scalar (also known as scalar curvature) is a scalar quantity defined at each point of the Riemann space [25]. Once again, to better understand what Riemann space is, it is a manifold where we can measure angles and distance of tangential vectors (one of these manifolds is for example Euclidean space mentioned in 2.2.2).

Ricci scalar is also defined as a trace of Ricci curvature tensor and can be written in Einstein's notation as

$$R = g^{\mu\nu} R_{\mu\nu} = R_a^a. \quad (2.8)$$

2. GENERAL THEORY OF RELATIVITY

It can also be written in term of Christoffel symbols as

$$R = g^{\mu\nu} (\Gamma_{\mu\nu,\lambda}^{\lambda} - \Gamma_{\mu\lambda,\nu}^{\lambda} + \Gamma_{\mu\nu}^{\sigma} \Gamma_{\lambda\sigma}^{\lambda} - \Gamma_{\mu\lambda}^{\sigma} \Gamma_{\nu\sigma}^{\lambda}), \quad (2.9)$$

where the notation $\Gamma_{\mu\nu,\lambda}^{\lambda}$ means the same as $\partial_{\lambda} \Gamma_{\mu\nu}^{\lambda}$.

2.2.4 Cosmological constant

The last component on the left side of the equation is metric $g_{\mu\nu}$ multiplied by cosmological constant Λ . This constant, said AE, was the "biggest blunder" in his work [25]. The constant at this point has many forms and is used in many variations of EFE. It might be strange that a constant can have many forms but the changes are not random. The main goal of the cosmological constant is to make our universe stationary and, within many models of the universe that exist, each one requires a different value.

2.2.5 Constants

The first component on the right side of the equation is a fraction made out of constants. In literature about GTR, you can usually find it labeled as Einstein's gravitational constant κ where

$$\kappa = \frac{8\pi G}{c^4}. \quad (2.10)$$

Newtonian constant of gravitation

The Newtonian constant of gravitation G (also used \varkappa) is a physical constant usually used in Newton's law of universal gravitation which in its scalar form is given as

$$F = G \frac{m_1 m_2}{r^2}. \quad (2.11)$$

Its value is $G = 6.674 \times 10^{-11} \text{ N m}^2 \text{ kg}^{-2}$.

Speed of light

As mentioned in chapter 2.1, c is a constant speed of light defined by AE in his paper on STR. Once again, we will mention its value as $c = 299792458 \text{ m s}^{-1}$.

2.2.6 Energy-momentum tensor

The last term of EFE is the Energy-momentum tensor $T_{\mu\nu}$ which describes the matter distribution. If we raise the indices in this tensor, we can construct it from the following equation,

$$T^{\mu\nu} = (\epsilon + p) u^\mu u^\nu - p g^{\mu\nu}. \quad (2.12)$$

In this equation, $\epsilon = \rho c^2$ is the energy density, (ρ is the density of matter), p is the scalar pressure, $u^\mu u^\nu$ is the tensorial product of the 4-velocities in an arbitrary coordinate system, and $g^{\mu\nu}$ is the metric. This product helps us to get all matrix components of the tensor $T^{\mu\nu}$ as seen in (2.13) with explicit formulas for the components in (2.14),

$$T^{\mu\nu} = \begin{pmatrix} T^{00} & T^{01} & T^{02} & T^{03} \\ T^{10} & T^{11} & T^{12} & T^{13} \\ T^{20} & T^{21} & T^{22} & T^{23} \\ T^{30} & T^{31} & T^{32} & T^{33} \end{pmatrix}, \quad (2.13)$$

$$\begin{aligned} T^{00} &= (\epsilon + p) u^0 u^0 - p = \gamma^2 (\epsilon + \beta^2 p), \\ T^{0i} = T^{i0} &= (\epsilon + p) u^0 u^i = \frac{\gamma^2}{c} (\epsilon + p) u^i, \\ T^{ij} &= (\epsilon + p) u^i u^j + p \delta^{ij} = \frac{\gamma^2}{c^2} (\epsilon + p) u^i u^j + p \delta^{ij}, \end{aligned} \quad (2.14)$$

where i, j now take the values 1, 2, 3, $\beta = u/c$, $\gamma = (1 - u^2/c^2)^{-1/2}$ is the Lorentz factor, and δ^{ij} is the Kronecker delta. In equations (2.14), behind the tensor, a new variable appears which is just a different form of a 4-velocity written as $u^\mu = \gamma (c, \vec{u})$, where c is the speed of light and \vec{u} is a 3-velocity.

For further explanation of the matrix components, we define T^{00} as the energy density of particles in the matter, T^{0i} and T^{i0} as the energy flux $\times c^{-1}$ in the i -direction (or the momentum density $\times c$ in the i -direction) and T^{ij} as the rate of flow of the i -components of momentum per unit area in the j -direction. This definition of the matrix components is the reason for the name energy-momentum tensor [25].

3 Answering the question about analysis

This chapter is the start of the statistical part of this thesis:

Our goal in this part is to analyze three of the most significant detections of GWs. To be more precise, GW150914, detected on 14th September 2015 by LIGO just after upgrading the detector via project aLIGO in the first observation run (O1), GW170814, detected on 14th August 2017 by LIGO and Virgo collaboration in the second run (O2), and last but not least GW170817 detected three days later on 17th August 2017 also by LIGO and Virgo collaboration in the second run (O2), and plot their waveforms.

3.1 Why are we doing the analysis?

Before we start, we should think about if and how this analysis benefits us as physicists and as a society. Usually, we (as astronomers) observe the universe by electromagnetic radiation (ER - ex.: X-rays, visible light, radio and microwaves, etc.) which gives us information and a specific view of the universe (even if the view is different from scientist to scientist, they are still very much complementary).

The GWs, however, are not of electromagnetic character and they are fundamentally unrelated to ER which gives us a new instrument to identify the universe. It is (as the name of this thesis indicates) a new window into space. Thanks to them, we observe space through ripples in a "sheet" of space-time and let us "see" the most distant parts of the universe. Of course, we can observe far Cosmos thanks to some of our most powerful telescopes that work on ER but some discrepancies can be resolved by GW observation. GWs almost do not interact with matter (on the other hand ER can be absorbed, reflected, etc.). Hence, they are better candidates for observing "the past" because, on their way to us, most of the GW does not fade away. They still carry information about the event without "losing" information and without distortion. [27]

Of course, GWs are not the "perfect tool" for discovering all that is in the Cosmos. They come to us as a weak signal that a person cannot feel. We need extremely perceptive detectors (as we mentioned in

section 1.3.3, there had to be many upgrades of the original detectors, and we are still working on better equipment) because we have to subtract the influence of mechanical waves and other disturbances here on Earth (especially seismic quakes or thermal noise) that can be interfering with the signal of GWs. We are aiming to better solve these issues by building detectors underground (ex.: KAGRA and Einstein Telescope in section 1.3.3) where we can much more efficiently isolate them from seismic waves and anthropogenic perturbations, or we are trying to send detectors to space (LISA in section 1.3.3) where there are no significant factors that would bring noise into the signal.

Still, even if GWs are somehow a "fixer-upper", so are the other ways to observe the universe. To conclude, we as a society are curious and will use and study anything new that is given to us just because of the question "What if...?".

3.2 How to analyze GWs data

3.2.1 Where we got the means used for analysis?

This thesis's main goal is to understand the issues associated with calculations of an accurate theoretical function that we can later compare to real data from GWOSC. The point of this subsection is to derive the formulas we need for analysis. Some formulas in this section will be taken as "fixed", meaning we will not be discussing where they came from; they have their stated form for the sake of the length and clarity of this thesis. Of course, there is no way formulas can just "come out of the blue" so we will be referencing textbook *Gravitational Waves: Volume 1: Theory and Experiments* as our main source [28].

Before anything else, we will write down our "foundation stone" a quadrupole radiation formula, first derivated by AE, which links total energy release and quadrupole moments (3.1). This is not the real foundation stone, but it will be ours. This equation needed to be derived from something but unfortunately this "something" it is beyond the scope of this thesis, therefore we will not be mentioning the origins.

$$\frac{dE_{\text{gw}}}{dt} = \frac{G}{5c^5} \langle \ddot{Q}_{ab} \ddot{Q}^{ab} \rangle, \quad (3.1)$$

where on the left-hand side is a time derivation of energy or the total energy release (later labeled as L_{gw} as the GWs' Luminosity) and on the right-hand side \ddot{Q}_{ab} and \ddot{Q}^{ab} are third derivatives of quadrupole moments that take the form of tensors, where the different positions of the indexes mean they are inverse forms of each other (in our case it does not matter because they are identical as will be derived later and shown via formulas (3.12)), G is Newton's gravitational constant, and c is a speed of light.¹

As our "cement", we must define what we will use the formula (3.1) for and how to expand it. We already mentioned that we would work with two detections of GWs (mentioned in subsection 1.3.3 and at the beginning of this chapter 3). These GWs were created by mergers of two stellar-mass black holes in the case of GW150914 and GW170814, and by binary neutron star merger in the case of GW170817. In all these cases they are binary system with the center-of-mass coordinates on a 2D xy plane. In our case, we will call the system "binary star" or BS for short in general.

The BS has fixed parameters, which are:

1. Masses of the stars m_1 and m_2 , total mass M , and a reduced mass μ ,

$$M = m_1 + m_2, \quad \mu = \frac{m_1 m_2}{m_1 + m_2}. \quad (3.2)$$

2. Separation of the stars a .

3. Angular frequency

$$\Omega = \sqrt{\frac{GM}{a^3}}. \quad (3.3)$$

4. Total orbital energy

$$E_{\text{orb}} = \frac{1}{2} (m_1 a_1^2 + m_2 a_2^2) \Omega^2 - \frac{Gm_1 m_2}{a} = -\frac{G\mu M}{2a}. \quad (3.4)$$

1. As you will see, there are reoccurring constants that are used repeatedly, this is why there is the table 3.1 in section 3.2.3 with all of them covered for clarity. They can also be found in the section Index 5.

3. ANSWERING THE QUESTION ABOUT ANALYSIS

In equation (3.4), we simplified the term in brackets as μa^2 by deriving this term from the moment of inertia by setting the coordinates of the central mass as zero. This is, exactly, why we defined our BS in the center-of-mass coordinates; to make it simpler. Thanks to this and to the choice of the coordinate system to make our BS move only in xy plane (meaning the coordinate z is always zero), we can define the coordinates of the circular motion as

$$x_0(t_{\text{ret}}) = R \cos \Omega t_{\text{ret}}, \quad y_0(t_{\text{ret}}) = R \sin \Omega t_{\text{ret}}, \quad z_0(t_{\text{ret}}) = 0. \quad (3.5)$$

We can also derive components of the already mentioned quadrupole moment tensor. We will implicitly implement equations (3.5) into the conventionally defined quadrupole moment tensor of the energy density of the source,

$$q_{ij}(t) = \int y^i y^j T^{00}(t, \mathbf{y}) d^3y. \quad (3.6)$$

In (3.6), we can see the term T^{00} which we know from subsection 2.2.6 is the first component of the energy-momentum tensor. For the formulation of the T^{00} term, we also need the trajectories of the objects A and B from our BS which are defined as

$$x_A^1 = R \cos \Omega t, \quad x_A^2 = R \sin \Omega t, \quad (3.7)$$

$$x_B^1 = -R \cos \Omega t, \quad x_B^2 = -R \sin \Omega t. \quad (3.8)$$

Now we can write the T^{00} term explicitly as

$$T^{00}(t, \mathbf{x}) = M \delta(x^3) \left[\delta(x^1 - R \cos \Omega t) \delta(x^2 - R \sin \Omega t) + \delta(x^1 + R \cos \Omega t) \delta(x^2 + R \sin \Omega t) \right], \quad (3.9)$$

where x^1, x^2 , and x^3 are components of the vector \mathbf{x} .

The explicit entry of the components, their second and third derivatives as functions of retarded time (a time when the field began to

propagate from the point where it was emitted to an observer) are

$$\begin{aligned} q_{11}(t_{\text{ret}}) &= \mu R^2 \cos^2 \Omega t_{\text{ret}}, \\ q_{22}(t_{\text{ret}}) &= \mu R^2 \sin^2 \Omega t_{\text{ret}}, \\ q_{12}(t_{\text{ret}}) &= \mu R^2 \sin \Omega t_{\text{ret}} \cos \Omega t_{\text{ret}}, \end{aligned} \quad (3.10)$$

$$\begin{aligned} \ddot{q}_{11}(t_{\text{ret}}) &= -2\mu R^2 \Omega^2 \cos 2\Omega t_{\text{ret}}, \\ \ddot{q}_{22}(t_{\text{ret}}) &= 2\mu R^2 \Omega^2 \cos 2\Omega t_{\text{ret}}, \\ \ddot{q}_{12}(t_{\text{ret}}) &= -2\mu R^2 \Omega^2 \sin 2\Omega t_{\text{ret}}, \end{aligned} \quad (3.11)$$

$$\begin{aligned} \ddot{\ddot{q}}_{11}(t_{\text{ret}}) &= 4\mu R^2 \Omega^3 \sin 2\Omega t_{\text{ret}}, \\ \ddot{\ddot{q}}_{22}(t_{\text{ret}}) &= -4\mu R^2 \Omega^3 \sin 2\Omega t_{\text{ret}}, \\ \ddot{\ddot{q}}_{12}(t_{\text{ret}}) &= -4\mu R^2 \Omega^3 \cos 2\Omega t_{\text{ret}}, \end{aligned} \quad (3.12)$$

where $q_{12} = q_{21}$ thanks to the symmetry of the tensor while other components vanish. The matrix will look as follows,

$$\ddot{\ddot{q}}_{ij}(t_{\text{ret}}) = 4\mu R^2 \Omega^3 \begin{pmatrix} \sin 2\Omega t_{\text{ret}} & -\cos 2\Omega t_{\text{ret}} & 0 \\ -\cos 2\Omega t_{\text{ret}} & -\sin 2\Omega t_{\text{ret}} & 0 \\ 0 & 0 & 0 \end{pmatrix}_{ij}. \quad (3.13)$$

The 3×3 tensor that will form from the components of (3.13) is traceless, meaning that the trace of the matrix is zero (can be easily verified by the definition of the trace).

Plugging the components from (3.12) to the Einstein's quadrupole radiation formula (3.1), we will get

$$L_{\text{gw}} = \frac{32G\mu^2 R^4 \Omega^6}{5c^5} = \frac{32G^4 \mu^2 M^3}{5c^5 R^5}, \quad (3.14)$$

where the additional parameters emerged from the substitution of all the products of the corresponding elements of two identical matrices (3.13) into the formula (3.1). As we mentioned, the luminosity L_{gw} is stated as a time derivation of energy. The BS loses energy by emitting gravitational radiation, so for the system to remain in equilibrium, the

distance between the components of the BS needs to decrease. From (3.14), we can get the rate of the two bodies' distance shrinking,

$$L_{\text{gw}} = -\frac{dE_{\text{orb}}}{dt} = -\frac{G\mu M}{2R^2} \frac{dR}{dt}. \quad (3.15)$$

For better understanding, we will rearrange the equation to express the rate of shrinking, so it is

$$\frac{dR}{dt} = -\frac{64G^3\mu M^2}{5c^5 R^3}. \quad (3.16)$$

With the knowledge of decreasing orbital distance of the two bodies in BS, we can express the frequency increase as

$$\frac{\dot{f}}{f} = \frac{\dot{\Omega}}{\Omega} = -\frac{3\dot{R}}{2R}, \quad (3.17)$$

where Ω is an angular frequency defined in (3.3) and $\dot{\Omega}$ is its time derivative. Therefore, we can introduce an initial or the present separation R_{init} and then, from equation (3.16), the BS will merge in the GW inspiral time (see the following equation (3.18)). The t_{GW} depends on how we choose our initial separation R_{init} , meaning that we can choose an orbital distance long time before the collision or closer to the time of merger,

$$t_{\text{GW}} = -\frac{5c^5}{64G^3\mu M^2} \int_{R_{\text{init}}}^0 R^3 dR = \frac{5c^5 R_{\text{init}}^4}{256G^3\mu M^2}. \quad (3.18)$$

As long as $\dot{\Omega} \ll \Omega^2$, we are in the quasi-circular motion regime (almost but not quite circular motion in a human language).

We can also see from (3.17) that as long as this inequality condition is fulfilled, $|\dot{R}|$ is much smaller than the tangential orbital velocity $V_\phi = R\Omega$ (derivation: $\dot{R} = -\frac{2}{3}R\frac{\dot{\Omega}}{\Omega} = -\frac{2}{3}R\Omega\frac{\dot{\Omega}}{\Omega^2} = -\frac{2}{3}V_\phi\frac{\dot{\Omega}}{\Omega^2}$) which means the approximation of a circular orbit with a slowly varying radius is then applicable.

Now, as we established our BS earlier on page 23, we can define formulas for GW polarisation amplitudes (3.19) and their explicit form (3.20), [28]

$$h_+(t, \mathbf{z}) = \frac{G}{c^4 r} (\ddot{q}_{11} - \ddot{q}_{22}), \quad h_\times(t, \mathbf{z}) = \frac{2G}{c^4 r} \ddot{q}_{12}, \quad (3.19)$$

$$h_+(t, \mathbf{n}) = \frac{4G\mu R^2 \Omega^2}{c^4 r} \left(\frac{1 + \cos^2 \theta}{2} \right) \cos(2\Omega t_{\text{ret}} + 2\phi), \quad (3.20)$$

$$h_\times(t, \mathbf{n}) = \frac{4G\mu R^2 \Omega^2}{c^4 r} \cos \theta \sin(2\Omega t_{\text{ret}} + 2\phi). \quad (3.21)$$

Now, as you have noticed, there is an orbital frequency Ω as well as two angles θ and ϕ . All those relations can be substituted in terms of the frequency f of GWs (that is twice the orbital frequency). With our approximation of circular orbit (where $\Omega \Delta t_{\text{ret}} = \Delta \phi$), the origin of time can be shifted so that we get the introduced form of (3.20), where $\Omega t_{\text{ret}} + \phi \rightarrow \Omega t_{\text{ret}}$, as

$$h_+(t, \mathbf{n}) = \frac{4G\mu R^2 (\pi f)^2}{c^4 r} \left(\frac{1 + \cos^2 \theta}{2} \right) \cos(2\pi f t_{\text{ret}}), \quad (3.22)$$

$$h_\times(t, \mathbf{n}) = \frac{4G\mu R^2 (\pi f)^2}{c^4 r} \cos \theta \sin(2\pi f t_{\text{ret}}). \quad (3.23)$$

With this newly adjusted form, we can easily see that if we would observe the GWs pole-on ($\theta = 0$), the amplitudes are identical. At the same time, the phase is shifted by $\pi/2$, meaning the wave is circularly polarised, whereas if we observe the system equator-on ($\theta = \pi/2$), the h_\times is equal to zero and h_+ is of half magnitude compared to the pole-on observed case, and the wave is linearly polarized.

For further consideration, we take equation (3.15) and modify it by plugging it in the definition of $\frac{dR}{dt}$ (3.16) (which is actually \dot{R}) and in the definition of Ω (3.3) (where the a is now R),

$$\dot{\Omega} = -\frac{3\Omega}{2R} \dot{R} = \frac{96G^{7/2} \mu M^{5/2}}{5c^5 R^{11/2}} = \frac{96G^{5/3} (\mu M^{2/3}) \Omega^{11/3}}{5c^5} \quad (3.24)$$

We now rearrange the equation (3.24) to express an explicit mass containing term (the product in brackets $\mu M^{2/3}$) in the dimension of mass $[g]$ which means, we need to raise this product to the power of $3/5$ and move it on one side. On the order side, we will get an equation containing Ω and its derivative $\dot{\Omega}$ observable due to the propagation of GWs. The equation now takes the form

$$\mu^{3/5} M^{2/5} = \left(\frac{5}{3} \right)^{3/5} \frac{c^3}{8G} \dot{\Omega}^{3/5} \Omega^{-11/5}. \quad (3.25)$$

Thanks to this set expression, we can now define the product on the left-hand side as a "chirp mass" \mathcal{M}_c . This form and its modified version only for primary and secondary masses, m_1, m_2 , now is

$$\mathcal{M}_c = \mu^{3/5} M^{2/5} = \frac{(m_1 m_2)^{3/5}}{(m_1 + m_2)^{1/5}}, \quad (3.26)$$

and can be measured from observation, thanks to the connection with objects' masses.

Implementing the chirp mass \mathcal{M}_c as a canonical quantity, we define "the chirp" as a rapid frequency increase \dot{f} . Taking our modified equation for $\dot{\Omega}$ (3.24) with the perception of the definition $\Omega = \pi f$ (meaning the angular frequency Ω is two times lower than the frequency f of the GWs), implying the wave has two peaks during one orbit, we can rewrite the equation as follows,

$$\dot{f} = \frac{96 c^3}{5 G \mathcal{M}_c} \left(\frac{G}{c^3} \pi f \mathcal{M}_c \right)^{8/3}. \quad (3.27)$$

By integrating the equation (3.27) as

$$\int \frac{df}{f^{11/3}} = \frac{96 c^3}{5 G \mathcal{M}_c} \left(\frac{G}{c^3} \pi \mathcal{M}_c \right)^{8/3} \int_t^{t_{\text{coal}}} dt, \quad (3.28)$$

we see that the frequency f formally diverges at the finite time \rightarrow the time of coalescence t_{coal} . We can now rewrite the equation of frequency f of GWs in terms of the time remaining until merger (time remaining to t_{coal}) as

$$f(t) = \frac{1}{\pi} \left(\frac{c^3}{G \mathcal{M}_c} \right)^{5/8} \left[\frac{5}{256 (t_{\text{coal}} - t)} \right]^{3/8}. \quad (3.29)$$

Now, inserting the equations (3.27) and (3.29) to the formula (3.17) will lead to an expression

$$\frac{\dot{R}}{R} = -\frac{2\dot{f}}{3f} = -\frac{1}{4(t_{\text{coal}} - t)}, \quad (3.30)$$

which we can integrate as the change of the radius according to time; it will give

$$\int_{R_0}^R \frac{dR}{R} = - \int_{t_0}^t \frac{dt'}{4(t_{\text{coal}} - t')},$$

that is, $R(t) = \left(\frac{t_{\text{coal}} - t}{t_{\text{coal}} - t_0} \right)^{1/4},$ (3.31)

where R_0 is the value of R at the initial time t_0 . Within this, we have to consider that after a long phase in which the R is decreasing relatively smoothly, there is a plunge phase where our approximation of a quasi-circular orbit is no longer valid.

By rearranging the equation (3.27), we can get expression for chirp mass \mathcal{M}_c as

$$\mathcal{M}_c = \frac{c^3}{G} \left(\frac{5}{96} \pi^{-8/3} f^{-11/3} \dot{f} \right)^{3/5},$$
 (3.32)

which we can substitute into the angle-independent part of equations either (3.22) or (3.23). We obtain (after some algebra and denominated of the general distance r to the luminosity distance D) the scaling amplitude h_0 as

$$h_0 = \frac{4}{D} \left(\frac{G\mathcal{M}_c}{c^2} \right)^{5/3} \left(\frac{\pi f}{c} \right)^{2/3}.$$
 (3.33)

In this lowest order Newtonian approximation, the amplitudes depend on object masses m_1 and m_2 only through the chirp mass \mathcal{M}_c . By simple inversion, we can thus calculate the luminosity distance D ,

$$D = \frac{4}{h_0} \left(\frac{G\mathcal{M}_c}{c^2} \right)^{5/3} \left(\frac{\pi f}{c} \right)^{2/3},$$
 (3.34)

which is a method of measuring the luminosity distance using only GW observables. This is extremely useful as an independent distance indicator in astronomy.

The amplitude of the emitted GWs depends on the angle between the line of sight and the axis of angular momentum; that's why the formulas for amplitudes (3.22) and (3.23) contain angular factors. Thanks

to this, we can also say that the relative strength of the two polarizations also depends on the angle, which is why it is the best when we actively use more than one detector for observing GWs. Not only we are more likely to detect them but it is more likely to get clearer and stronger signal which can help us to construct full waveform and deduce much more details about the orbit of the BS. Great example is the well-studied "the Hulse-Taylor pulsar" where we were able to deduct the time of merger, period change, masses of the two neutron stars that it consists of and how far the BS is.

3.2.2 Where to obtain data?

We now need to obtain data that we can analyze. All data used in this thesis are from GWOSC (Gravitational Wave Open Science Center). The GWOSC has a database of every detection of GWs to this day with classifications of the data types: pre-confident data released before the catalogization and confident data released in the catalog, which are supplied by worldwide detectors.

For this thesis, we will be using the data published in *A Gravitational-Wave Transient Catalog of Compact Binary Mergers Observed by LIGO and Virgo during the First and Second Observing Runs* (GWRC-1 for short). If labeled as confident, LIGO and Virgo marked them as relevant based on the correct determination of time of the detection and correct interval of frequency, to classify it as the real detection of GWs. In the GWTC-1-confident catalog, the classification of data is based on how long we want data around the event and in which interval of frequencies we want the strain time-series data to be sampled. For our use, we chose data detected within 32 seconds around the events with a sampling rate of 4096 Hz. [29]

3.2.3 What else is needed for calculations?

Now that we know how to calculate values of our needed parameters and where to find data of the mergers, all we need is to assign precise values of physical constants used in the formulas. We will use *SciPy* [30] and its package `scipy.constants`, where we can find values valid to many decimal places (depending on how well we, as a society, were able to measure them). As promised in section 3.2.1, in this paragraph

3. ANSWERING THE QUESTION ABOUT ANALYSIS

is a table with all the constants that occur in the formulas introduced and some of the unit conversions used. ²

Table 3.1: Overview of used constants and conversions.

	Value / Conversion
Parsec to meter	$1\text{pc} = 3.086 \times 10^{16} \text{ m}$
Solar mass to kilogram	$1M_{\odot} = 1.998 \times 10^{30} \text{ kg}$
Newton's gravitational constant	$G = 6.674 \times 10^{-11} \text{ m}^3 \cdot \text{kg}^{-1} \cdot \text{s}^{-2}$
Speed of light	$c = 299792458.0 \text{ m} \cdot \text{s}^{-1}$

We also need to establish the merger's qualities as discussed in section 3.2.1.

Table 3.2: Used parameters of mergers GW150914, GW170814, and GW170817.

	GW150914	GW170814	GW170817
t (s) (GPS)	1126259462.4	1186741861.5	1187008882.4
D (Mpc)	440^{+150}_{-170}	600^{+150}_{-220}	40^{+7}_{-15}
m_1 (M_{\odot})	$35.6^{+4.7}_{-3.1}$	$30.6^{+5.6}_{-3.0}$	$1.46^{+0.12}_{-0.10}$
m_2 (M_{\odot})	$30.6^{+3.0}_{-4.4}$	$25.2^{+2.8}_{-4.0}$	$1.27^{+0.09}_{-0.09}$

In the table 3.2 the quantities are t for a GPS time (Global Positioning System time) in seconds, D is a luminosity distance in Megaparsecs and $m_{1,2}$ are primary and secondary mass in solar masses.

2. Of course, we did not write the constant correctly to all of the decimal places that are known, this is just to grasp what the values approximately are. The accurate values used are available at the official website of *SciPy*.

4 Analysis and calculation of theoretical waveform

Now that all is ready, we can start processing data:

We used the most basic packages for plotting and basic mathematical calculations *Numpy*, *Matplotlib*, and already mentioned *SciPy*. Only packages that stand out are packages *ReadLigo* and *H5py*. These are used for reading the datasets used in this analysis. For measured data (MD for short), we used code from the tutorials made specifically by GWOSC to help us get through common data analysis. For this part, we got help from a tutorial "*SIGNAL PROCESSING WITH GW150914 OPEN DATA*" [31] and its updated version "*BINARY BLACK HOLE SIGNALS IN LIGO OPEN DATA*" [32]. Our version of the used code for analysis is listed in Appendix A.

4.1 GW150914

GW150914 is the first detection of gravitational waves, that confirmed explanation of GWs by GTR, so it is highly appropriate and suitable to analyze it first and show how we are doing it, so we can later apply it to the events GW170814 and GW170817.

4.1.1 Measured data

Before starting, let us remind ourselves that we worked with the MD from GWOSC. We were following the code in subsection A.1.2 which we adopted from the mentioned tutorials ([31] and [32]).

In figure 4.1, there are raw data plotted to show 10 seconds around the event (5 seconds before and 5 seconds after) for both aLIGO detectors H1 (in Hanford, Washington) and L1 (in Livingston, Louisiana). In this case, we can put them together because the data are not much different from each other (later we will slightly shift L1 data which will be mentioned again).

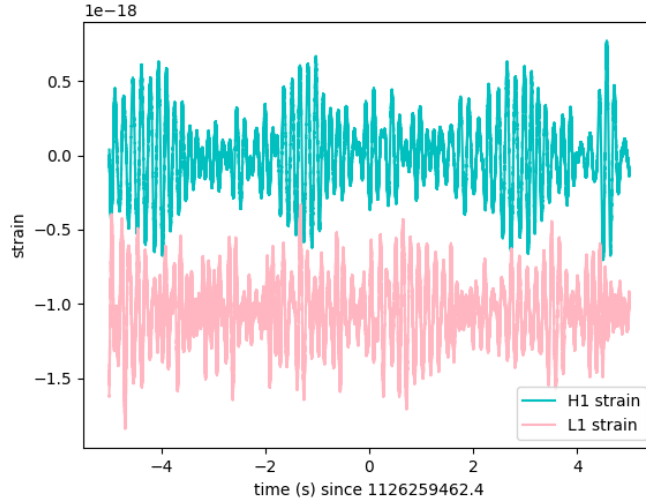


Figure 4.1: Raw Advanced LIGO strain data near GW150914.

The raw data mainly consist of low-frequency noise so we need to process them to see the signal, that is why we are going to whiten the data with Fast Fourier Transform (FFT for short) and Amplitude Spectral Density (ASD for short). The whitening is crucial in every data analysis in astrophysics. It is also very convenient because we do not need any information about the spectral lines so we only work with measured data. Whitening means, we are dividing the data by the noise amplitude spectrum. Thanks to that, we can better see the weak signals. Plotting the data in the Fourier domain will give us a picture of how the frequency contents of the data look. The ASDs are a way to visualize the frequency contents and represent the square root of the power spectral densities (PSDs), which are obtained by averaging the squares of the fast Fourier transforms (FFTs) of the data. Thanks to that, we can better extract the weak signals.

We plotted data in the frequency interval from 10 Hz to 2000 Hz because the data below this interval is not properly calibrated and even if they were, there is very high noise so we cannot extract the proper GWs strain there. On the other hand, the data cannot capture frequency above the Nyquist frequency (the highest achievable frequency) which can be expressed by a sampled signal as a $f_{\text{nyq}} = f/2$. This means

4. ANALYSIS AND CALCULATION OF THEORETICAL WAVEFORM

that our highest frequency is $f_{\text{nyq}} = 2048$ Hz which is not a problem because the GW150914 has a detectable range of 20 Hz to 300 Hz [31].

We are also bandpassing the data. By bandpassing, we are letting pass only frequencies of the chosen interval of frequencies and others are suppressed. As was mentioned in the paragraph above, our interval is from 20 Hz to 300 Hz. We also shifted the data from L1 by 7 ms so both H1 and L1 are lined up [31].³ The plotted ASDs and the whitened data are shown in figures 4.2 and 4.3

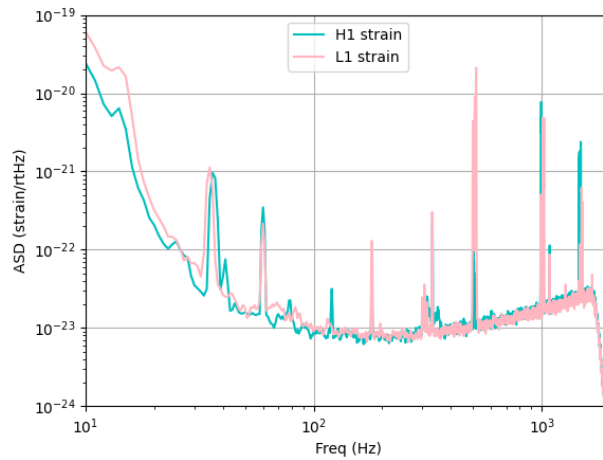


Figure 4.2: ASDs of Advanced LIGO data near GW150914.

Now we can already see an intensifying wave ready for the theoretical waveform (TW for short) to be plugged in.

3. In [31], they did not shift the data so the event is happening at the zero time, but later they shifted the non-relativistic form they are plugging in. For our convenience, we chose the opposite way and shifted the data so that later it is evident where our calculations took us.

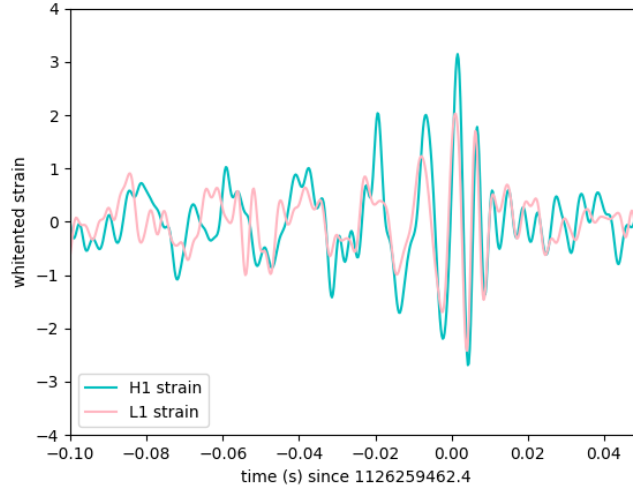


Figure 4.3: Whitened Advanced LIGO strain data near GW150914.

4.1.2 Theoretical waveform

Now that we whitened the data, we will plot our TW using the code in subsection A.1.3. For the TW, we used formulas (3.29) and (3.33) to calculate the frequency and the amplitude used in the wave function. As can be seen, we used the scaling amplitude h_0 (meaning we did not use the angular factors). We used it as an approximation so we do not need to calculate the angles. When we got our parameter, we simply plugged it into a basic formula describing the wave,

$$w = A \cos \omega t, \quad (4.1)$$

where $A = h_0$ and $\omega = 2\pi f$. We defined time t as an interval that corresponds to the time interval we used for whitened data so the TW and MD fit nicely with each other.

After calculations and plotting, while the silhouette of our TW looks nice when we plot it over MD, it does not fit quite well when we only use the values from table 3.2 without adding or subtracting the deviation; the collision corresponds and fits nicely but the farther we are from t_{coal} , there are some deviations. We tried many combina-

tions of values and uncertainties as seen in figures 4.4 and 4.5 before ending up with the version depicted in figure 4.6.

For the TW to fit like Cinderella's shoe, some tweaking was necessary. After trials and errors, we found out the luminosity distance D should be used with minus uncertainty (the uncertainty that is subtracted from the parameter's value), and masses $m_{1,2}$ with minus uncertainty and subtraction of $6.5 M_{\odot}$ which is quite the correction, as $6.5 M_{\odot}$ is in the primary star's mass almost $1/6$ and for the secondary star it is roughly $1/5$. We will comment more on that in the conclusion in the chapter 5.

4. ANALYSIS AND CALCULATION OF THEORETICAL WAVEFORM

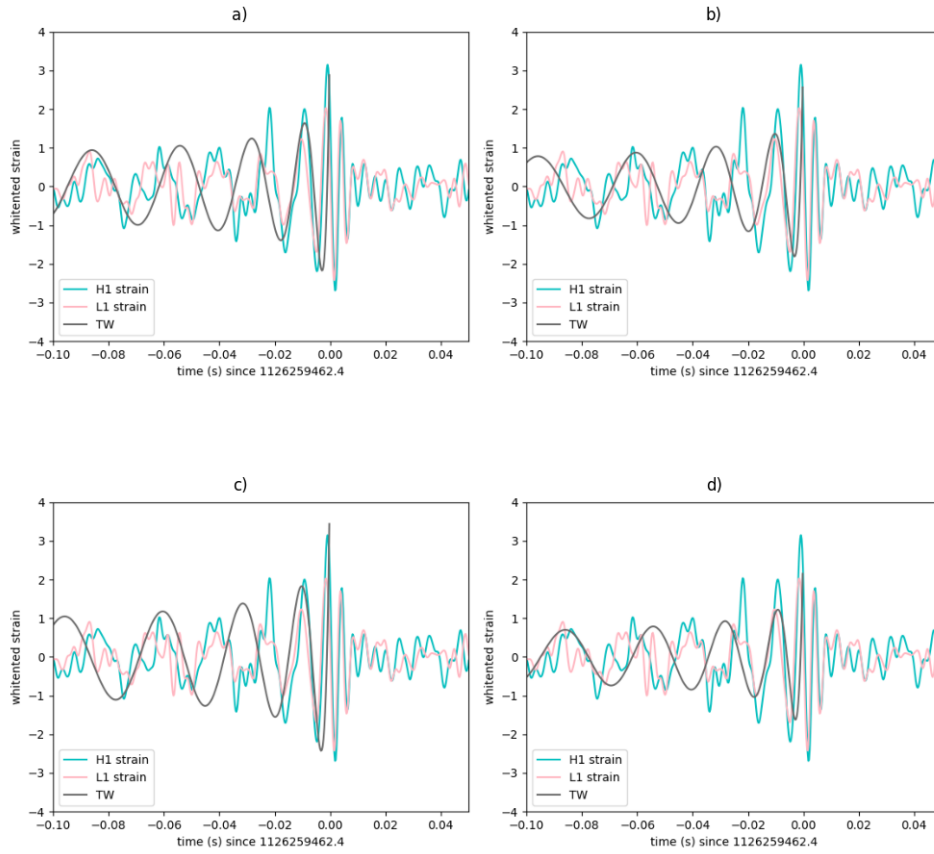


Figure 4.4: Comparing TW to the MD of GW150914 while changing the parameters from table 3.2: a) values without uncertainties, b) values while adding uncertainties, c) adding uncertainty only in luminosity distance, d) adding uncertainties to both masses.

4. ANALYSIS AND CALCULATION OF THEORETICAL WAVEFORM

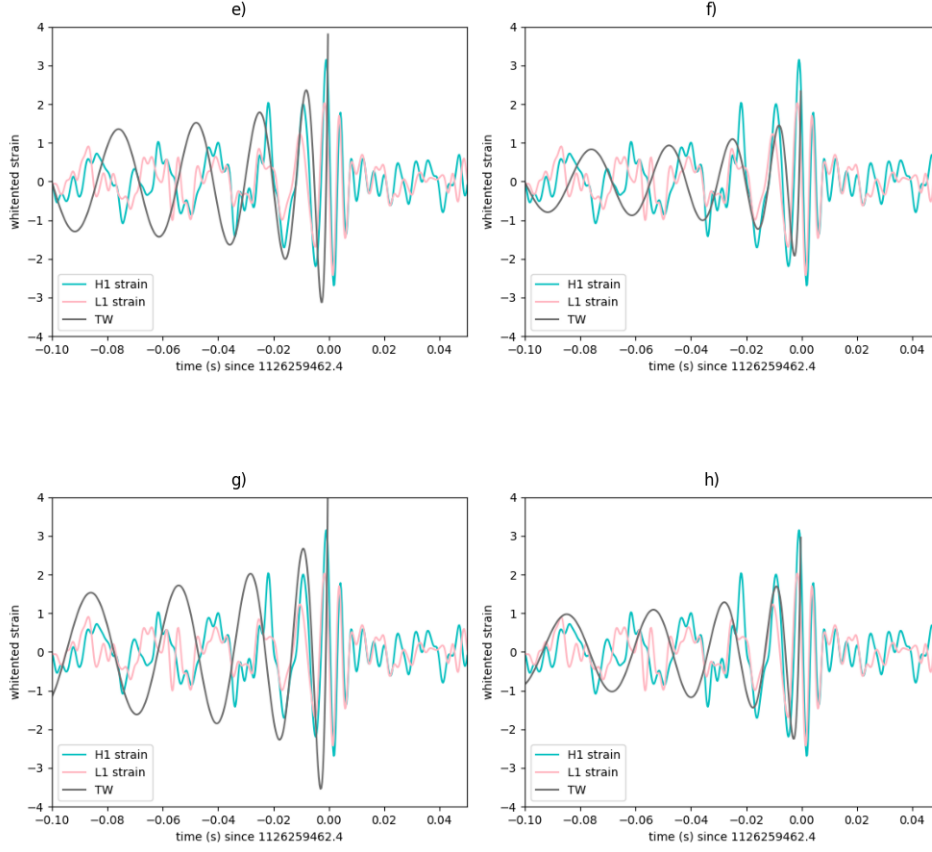


Figure 4.5: Comparing TW to the MD of GW150914 while changing the parameters from table 3.2: e) values while subtracting uncertainties, f) subtracting uncertainty only in luminosity distance, g) subtracting uncertainties to both masses, h) subtracting uncertainties from themselves ($D = 440 - 20$ Mpc, $m_1 = 35.6 + 1.6 M_\odot$, $m_2 = 30.6 - 1.4 M_\odot$).

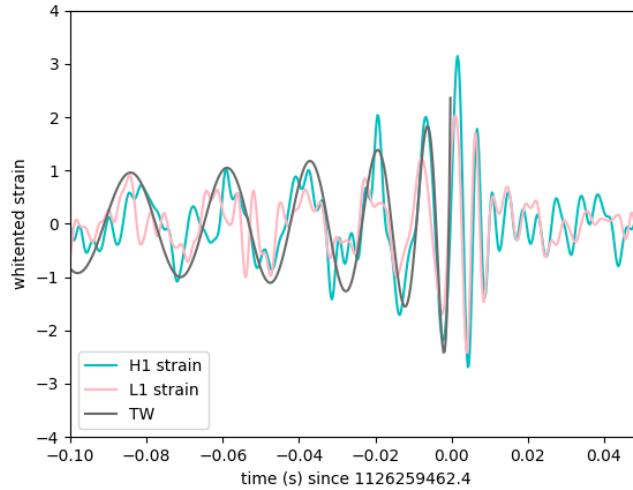


Figure 4.6: Final TW showcased on whitened strain data near GW150914.

4.1.3 Spectrograms

Lastly, let us plot a short time-frequency spectrogram with a color gradient displaying an amplitude corresponding to the frequency otherwise called "loudness" or "strength" of the signal (in our case the lighter the color is, the higher is the value of the amplitude). With these, we can obtain a visual representation of how the frequency varies with time. For comparison, we will be plotting both raw and whitened data. It might be obvious but just in the following case: we cannot plot both H1 and L1 together, although stated in subsection 4.1.1 that the H1 and L1 are not much different, in the case of spectrograms it is always better to do everything one by one.

On the spectrograms in figures 4.7 and 4.8, you can see very prominent horizontal lines at 500, 1000, and 1500 Hz; when we look back at the figure 4.2 you can see a correlation with the vertical lines on our ASDs graph. These lines are multiples of 500 Hz that are harmonics of the "violin modes" of the fibers holding the mirrors of the aLigo

4. ANALYSIS AND CALCULATION OF THEORETICAL WAVEFORM

interferometers. Also, we can see quite a lot of excess power below approx. 20 Hz [32].

The main focus should be on a very faint white line around zero time. This gives us a clue to where the "chirp" could be. At the end, the chirp will be there so let us zoom in and use whitened data to help us to see it better.

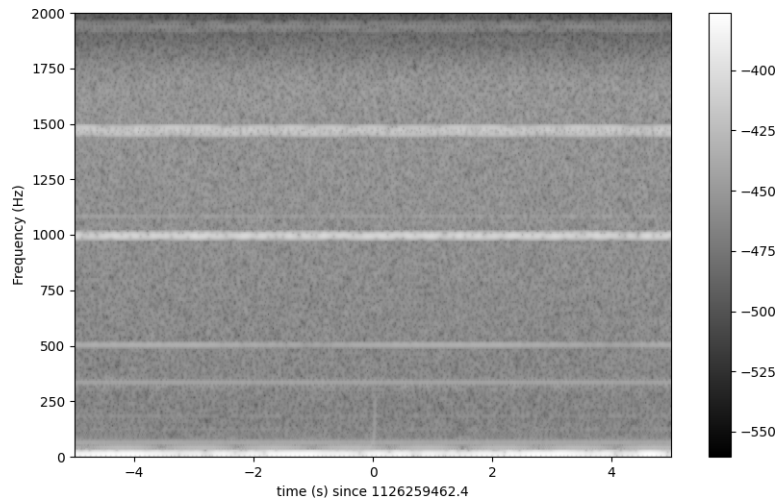


Figure 4.7: Time-frequency spectrogram of aLIGO H1 raw strain data near GW150914. The sense of the colorbar is explained at the start of the section 4.1.3.

4. ANALYSIS AND CALCULATION OF THEORETICAL WAVEFORM

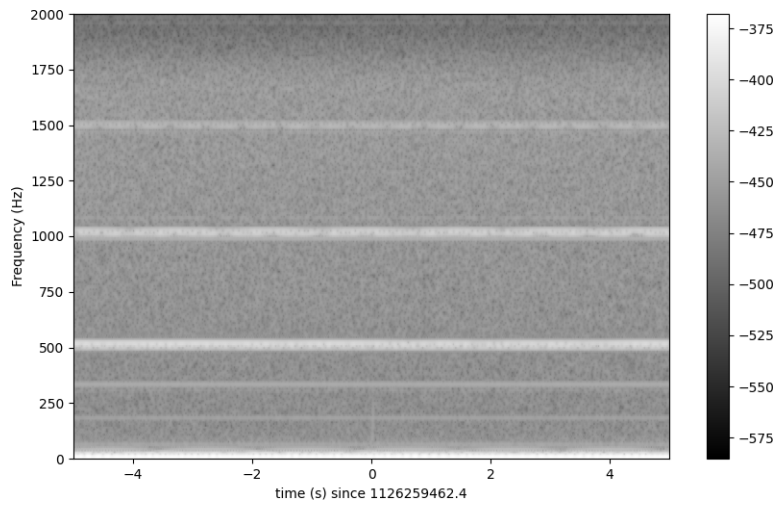


Figure 4.8: Time-frequency spectrogram of aLIGO L1 raw strain data near GW150914.

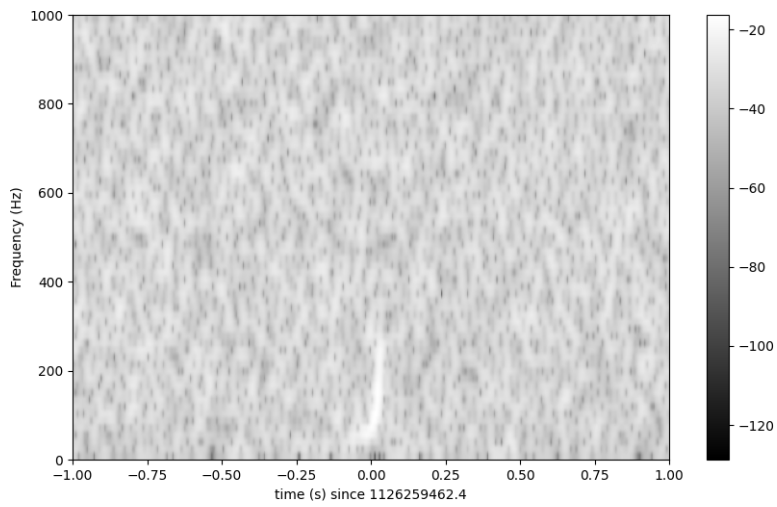


Figure 4.9: Time-frequency spectrogram of aLIGO H1 whitened strain data near GW150914.

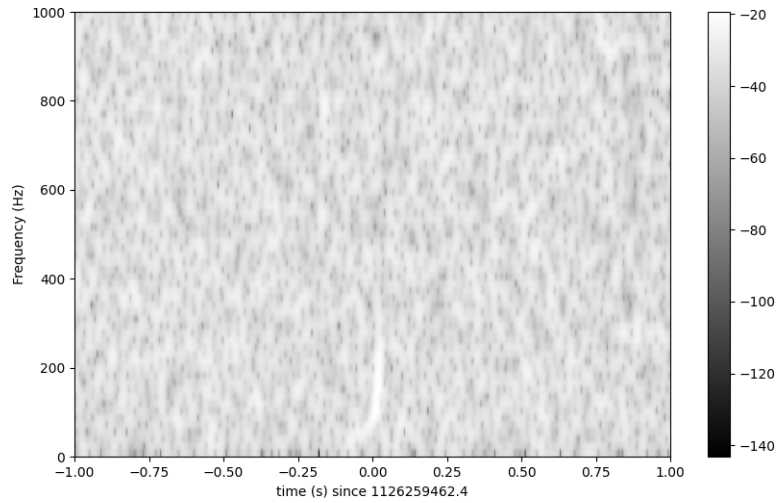


Figure 4.10: Time-frequency spectrogram of aLIGO L1 whitened strain data near GW150914.

Now, thanks to our intuition and zooming in on that faint line, the iconic "chirp" of the merger on the spectrograms in figures 4.9 and 4.10 is depicted as a bold white "whoosh". The figures show us the definition of chirp - the rapid frequency growth before the collision.

4.2 GW170814

Let us continue chronologically with GW170814. This detection was also "The first" with GWs because for the first time, GWs were detected by the all then operating detectors (meaning both detectors of aLigo and also Virgo, during the LVC)

4.2.1 Measured data

For this detection and later also for GW170817 (also mentioned at the beginning of the section 4.1), we essentially followed the same steps applied to the GW150914. Every detection of GWs is unique and different, therefore, we need to change some intervals and values. Even though we are using the same code, the version for this detection

4. ANALYSIS AND CALCULATION OF THEORETICAL WAVEFORM

will have its section in the appendix (A.2 with the code for the TW in subsection 4.2.2 and for spectrograms in subsection 4.2.3).

In the following order, we plotted the raw data, the ASDs, and the whitened data. For the raw data in figure 4.11, we see that the

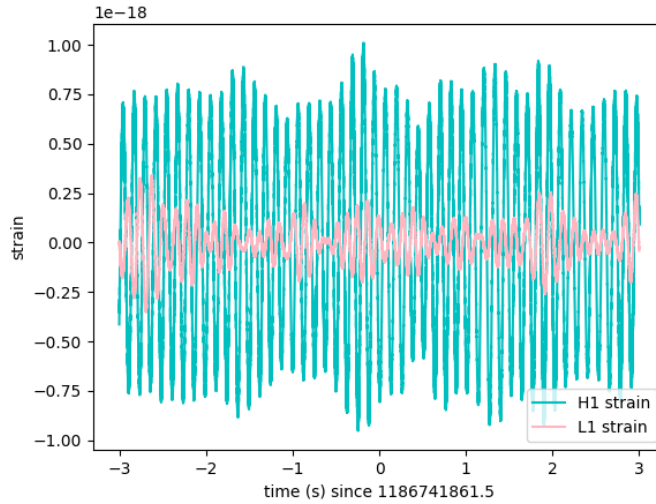


Figure 4.11: Raw Advanced LIGO strain data near GW170814.

Hanford detector H1 has a much bigger strain, but as we mentioned in the section 4.1 where we analyzed the GW150914; this data is not the best to look for signal without any "cleaning". As seen in 4.13, it did not influence the final whitened data when the standard approach without any tweaking was used. Also, we chose a smaller time interval so the peaks can be seen because if we decided to choose a longer one, it would look like some "data forest" which is even more confusing than the raw data itself, so let us keep it simple. Lastly, there is an evident difference from GW150914 which is that the signals overlap each other; at the first sight, it could look like the data is not beautifully separated as in the previous case and we were too lazy to do that, which is not true. About the data itself: we are not sure if it is caused by GWOSC or just by the nature of the data, but we will not be questioning the data anymore because all of the data are from the

4. ANALYSIS AND CALCULATION OF THEORETICAL WAVEFORM

GWTC-1-confident catalog and we are putting trust in the scientist that proclaimed them confident.

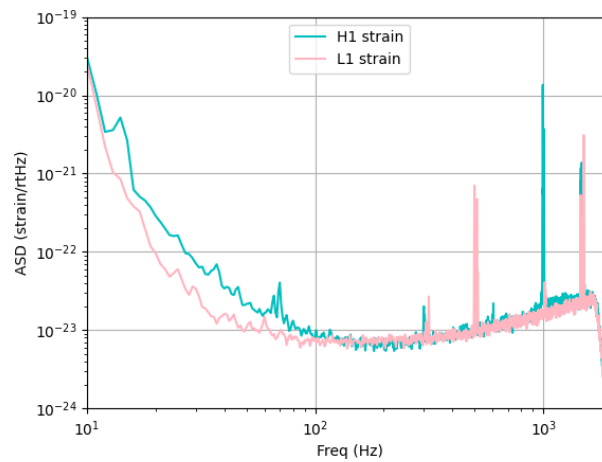


Figure 4.12: ASDs of Advanced LIGO data near GW170814.

When it comes to ASDs in figure 4.12, we can easily see the vertical lines that will copy to the spectrograms as horizontal lines as seen in figures 4.17 and 4.18. Thankfully, we did not need to change anything in case of frequency interval or Nyquist frequency here because we are still using the aLIGO data that were measured by the same detectors with the same parameters as GW150914.

4. ANALYSIS AND CALCULATION OF THEORETICAL WAVEFORM

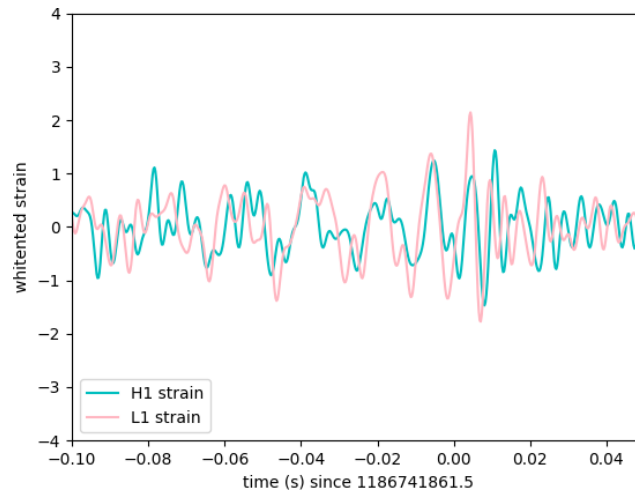


Figure 4.13: Whitened Advanced LIGO strain data near GW170814.

Final whitened data in figure 4.13 are not as clearly defined as in the previous case but we can still observe some "waviness" in there. After plugging in the TW, it will all come together.

4.2.2 Theoretical wavefunction

Now for the TW, we chose the corresponding data for this event from the table 3.2. While analyzing, we encountered the same problem as with GW150914, meaning we had to try out all the combinations of values and uncertainties as can be seen in figures 4.14 and 4.15. For all the other steps we did the same as with GW150914 meaning the calculation of parameters and plugging them into a basic wave equation. The final graph with both MD and TW is depicted in figure 4.24.

4. ANALYSIS AND CALCULATION OF THEORETICAL WAVEFORM

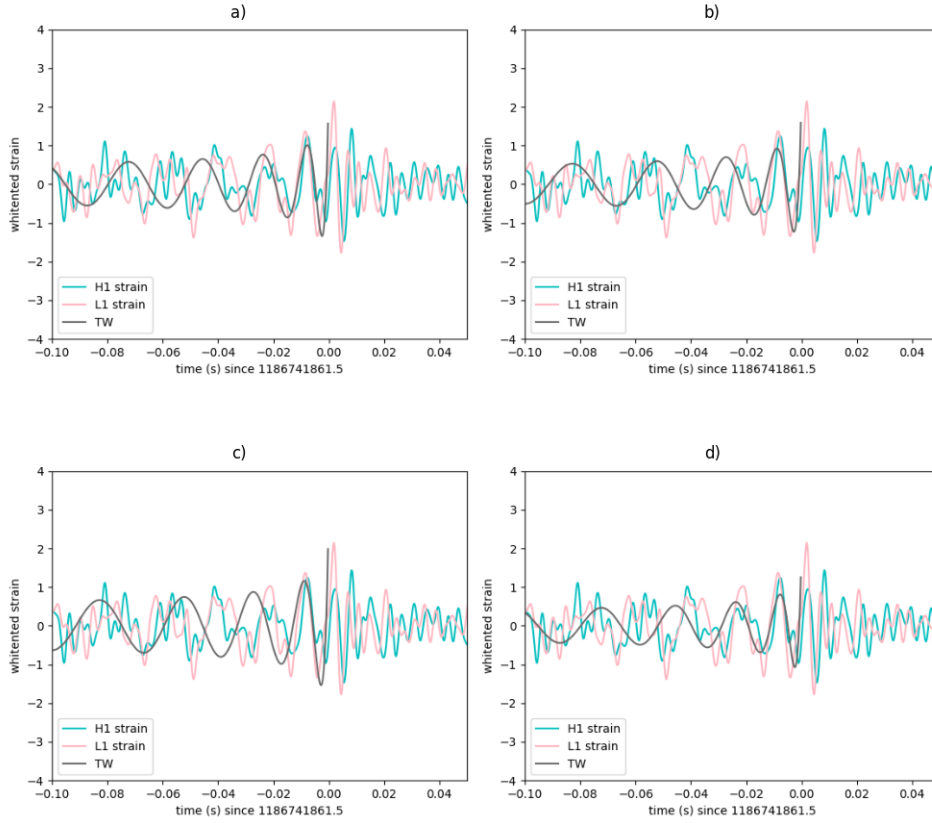


Figure 4.14: Comparing TW to the MD of GW170814 while changing the parameters from table 3.2: a) values without uncertainties, b) values while adding uncertainties, c) adding uncertainty only in luminosity distance, d) adding uncertainties to both masses.

4. ANALYSIS AND CALCULATION OF THEORETICAL WAVEFORM

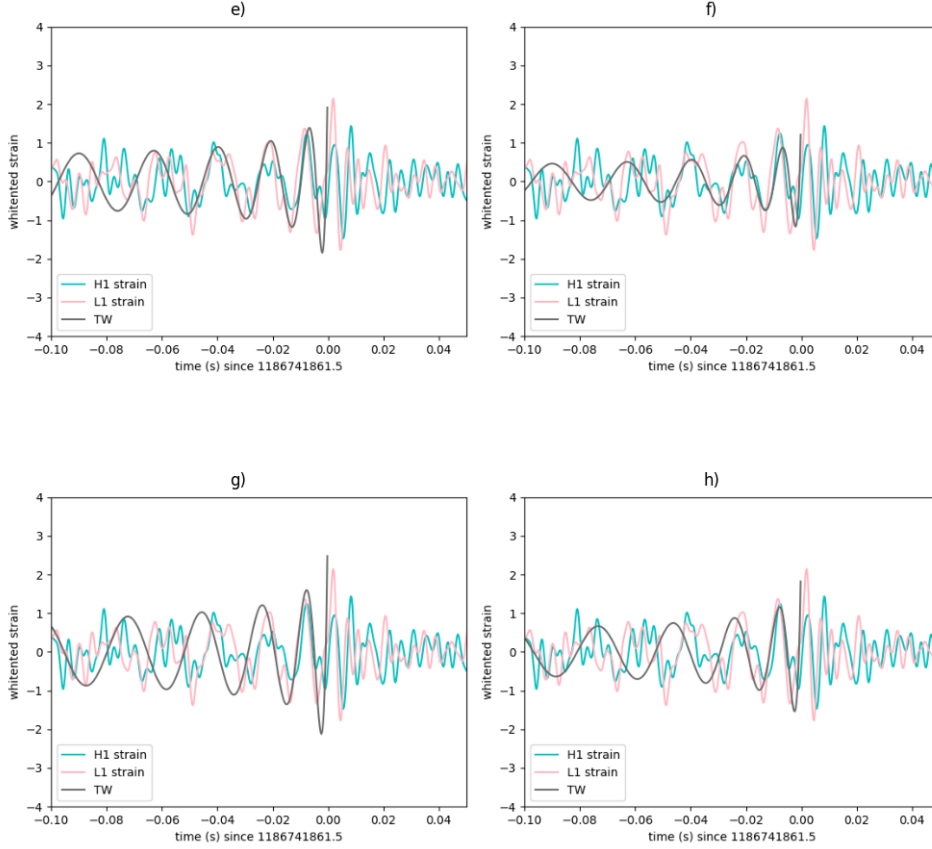


Figure 4.15: Comparing TW to the MD of GW170814 while changing the parameters from table 3.2: e) values while subtracting uncertainties, f) subtracting uncertainty only in luminosity distance, g) subtracting uncertainties to both masses, h) subtracting uncertainties from themselves ($D = 600 - 70$ Mpc, $m_1 = 30.6 + 2.6 M_\odot$, $m_2 = 25.2 - 1.2 M_\odot$).

As can be seen once again, none of the combinations were able to fit the MD data nicely so we needed to add corrections. This time, our correction applied to masses $m_{1,2}$ by adding $4.6 M_\odot$ while using all values from table 3.2 with the minus uncertainties. Whilst the TW fits

as snuggly as we were able to make it to, it is not of the best occurrence because a) it needed to be added without any previous reasoning (we did not do anything that explicitly needed this correction) and b) it is different from the GW150914 correction which could mean it is not a statistical error. We will discuss this matter later in the conclusions, in the chapter 5.

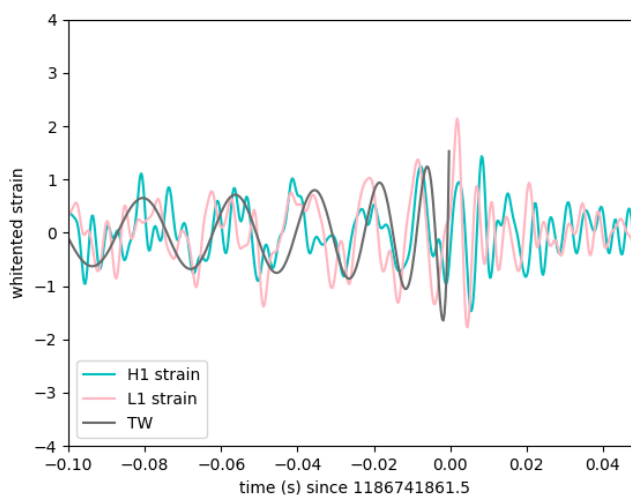


Figure 4.16: Final TW showcased on whitened strain data near GW170814.

4.2.3 Spectrograms

Lastly, let us look at the spectrograms. As we said earlier in the GW170814 analysis (4.2.1) in the raw data spectrograms in figures 4.17 and 4.18, we can see the ASDs vertical lines turned into horizontal lines and on x -axis when the time equals to zero, we can see small faint vertical line which as we know is a clue where the chirp is.

In the whitened data spectrograms, we can see once again the chirp as a white "whoosh" which is more defined in the case of the L1 detector in figure 4.20. There is a very wild-looking background for the H1 whitened data spectrogram in figure 4.17 so if we do not know

4. ANALYSIS AND CALCULATION OF THEORETICAL WAVEFORM

what we are looking at and what we are looking for, it would be a tough nut to crack.

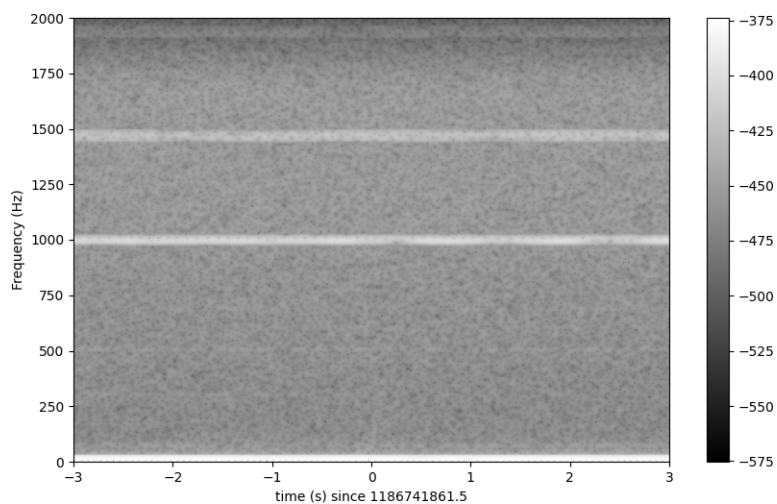


Figure 4.17: Time-frequency spectrogram of aLIGO H1 raw strain data near GW170814.

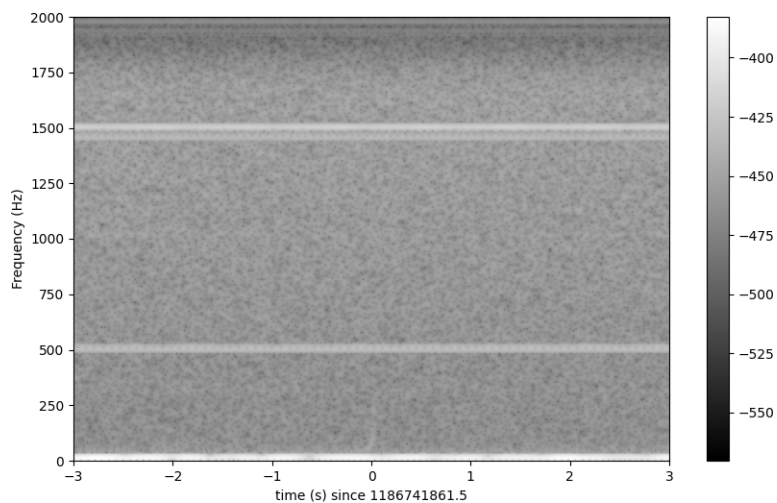


Figure 4.18: Time-frequency spectrogram of aLIGO L1 raw strain data near GW170814.

4. ANALYSIS AND CALCULATION OF THEORETICAL WAVEFORM

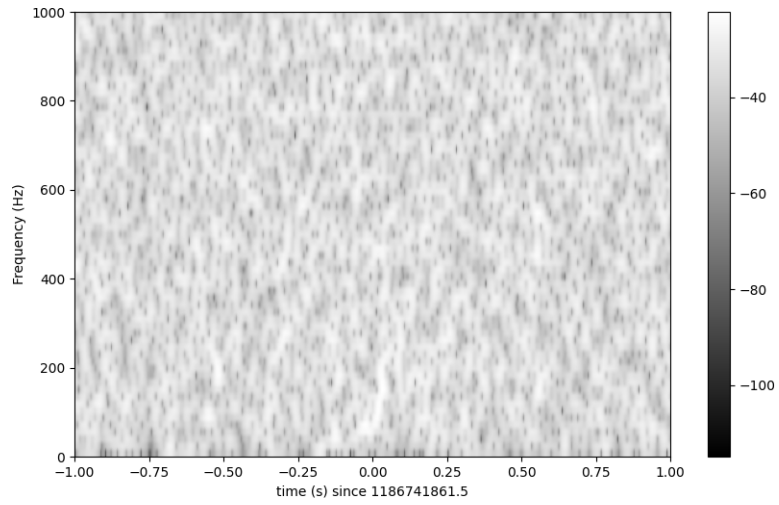


Figure 4.19: Time-frequency spectrogram of aLIGO H1 whitened strain data near GW170814.

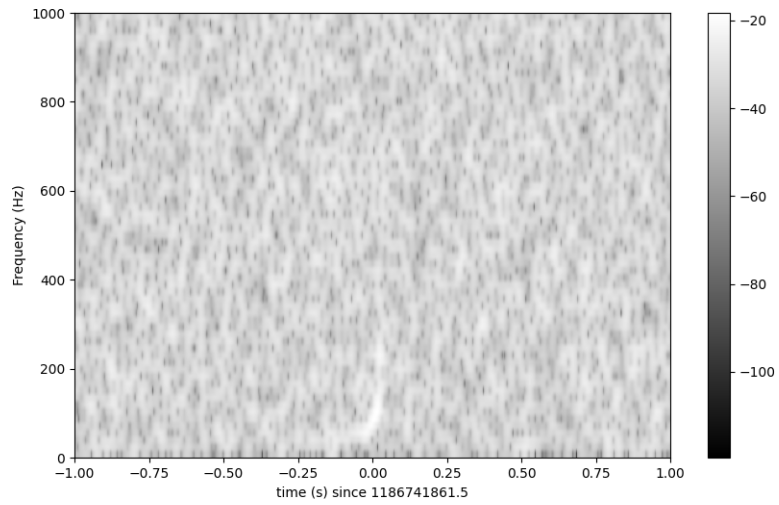


Figure 4.20: Time-frequency spectrogram of aLIGO L1 whitened strain data near GW170814.

4.3 GW170817

Last but not least (actually the "biggest" detection in terms of observation), we will analyze the detection of GW170817. This detection is important because it was not only detected via the GW detectors but also by gamma-ray detectors (and the following afterglows) thanks to the short gamma-ray burst that accompanied the GWs.

4.3.1 Measured data

As was done before, in this section would normally be an analysis of MD where we would showcase a progress from raw, quite nasty-looking data to pleasant wave formation in the whitened data. In this case, it is not possible. The data is very diverse when it comes to the datasets from each aLIGO detector and even when it comes to frequencies in the same dataset. This might be because it was a powerful signal compared to the time of quiescence and the fact that it was accompanied by the gamma-ray burst.

Even though this is the case, it would be a shame not to demonstrate how it turned out because it is still an analysis of the data. It might not be usable but at least it will show that not all things go the way we want and also it could serve as a reassurance for those who are racking their brains over this data and wondering where they went wrong. So, in the figures 4.21, 4.22, and 4.23, we can see our attempts to analyze the data.

At the first sight, the raw data in figure 4.21 looks somewhat like the GW170814 raw data pictured in figure 4.11. In both cases, we needed to choose a smaller time interval so it looks presentable, yet the outcomes are as different as chalk and cheese. Also in the case of GW170817, the chirp is shifted to $t = -1$ s. The same goes for the ASDs in figure 4.22 where we would not be able to tell if the data will end up in the same way as in our two previous attempts.

In figure 4.23, we see the problem. There is no way, we can bandpass the data in one time interval that would show us the big chirp detected on the L1 detector and simultaneously show the data detected on the H1 detector. In this thesis, we are trying to analyze the data so they can sit on each other and complete each other, so this data leads to no purpose. Even if we could successfully separate the data, there

4. ANALYSIS AND CALCULATION OF THEORETICAL WAVEFORM

would be more complications that we will mention in conclusions in the chapter 5.

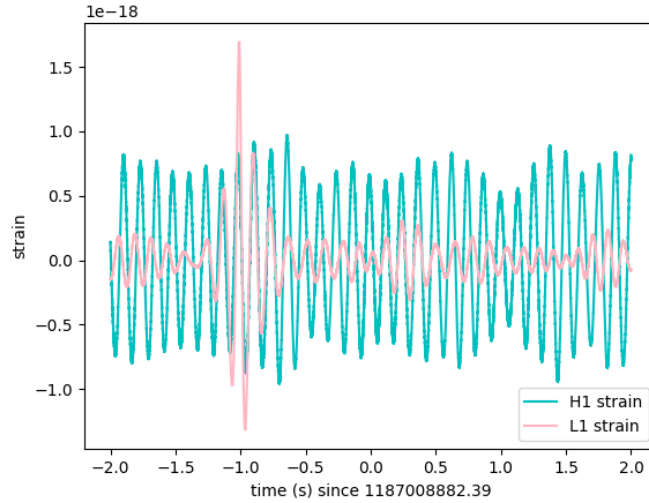


Figure 4.21: Raw Advanced LIGO strain data near GW170817.

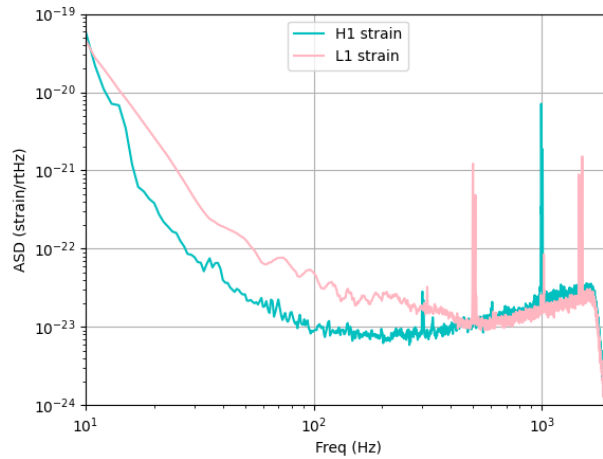


Figure 4.22: ASDs of Advanced LIGO data near GW170817.

4. ANALYSIS AND CALCULATION OF THEORETICAL WAVEFORM

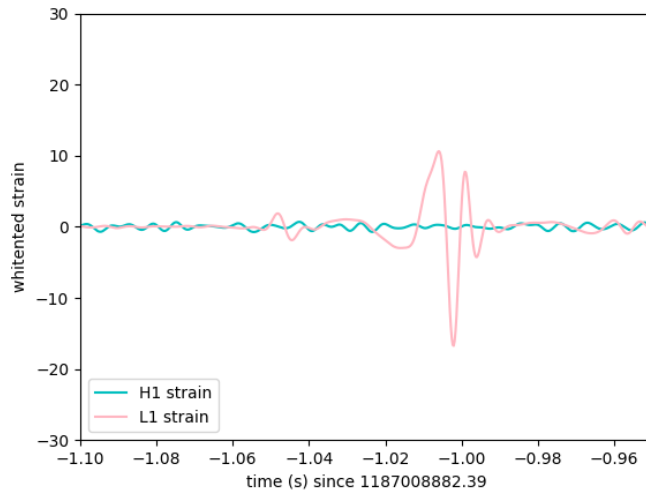


Figure 4.23: Whitened Advanced LIGO strain data near GW170817.

4.3.2 Theoretical waveform

This subsection is only to expose more of our fiasco, yet again, we think it is important to show this, so one can see all we did to try to make it all work.

Basically, in figure 4.24, we can see how inadequate is the TW on MD. We used the values from table 3.2 without using uncertainties. We did not include our trials as we did for GW150914 and GW170814 (subsections 4.1.2 and 4.2.2) because all of them were as ill-fitting as this one.

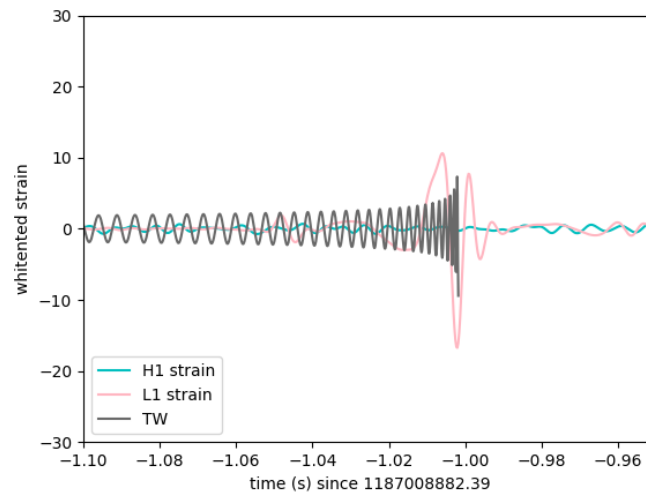


Figure 4.24: Final TW showcased on whitened strain data near GW170817.

4.3.3 Spectrograms

When it comes to the spectrograms, it is better. We can easily see the clues where the chirp should be and on the whitened data where the chirp is. Also, as said before in subsection 4.3.1, the chirp is not happening in time equal to zero but around $t = -1$ s.

4. ANALYSIS AND CALCULATION OF THEORETICAL WAVEFORM

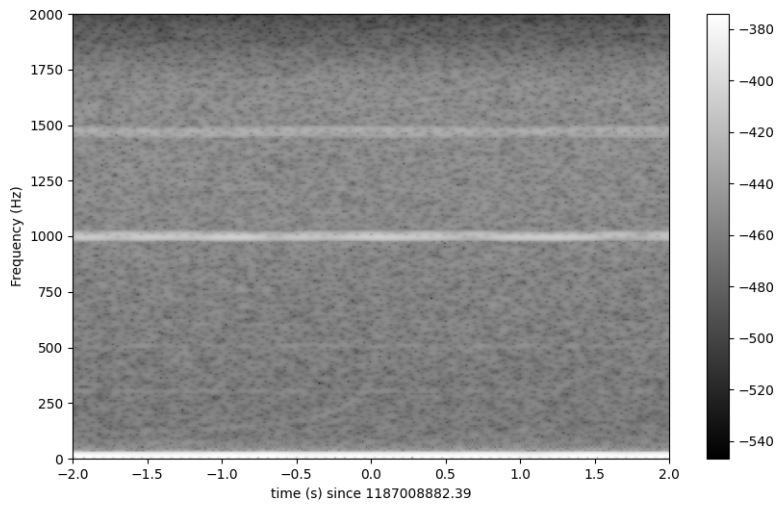


Figure 4.25: Time-frequency spectrogram of aLIGO H1 raw strain data near GW170817.

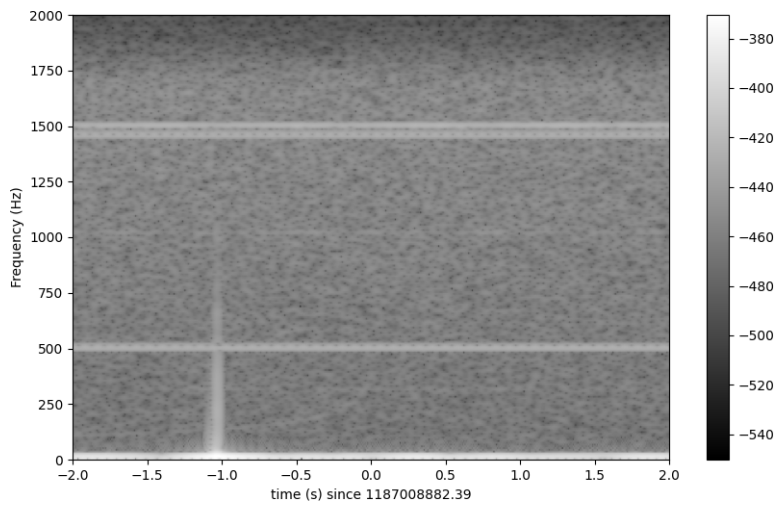


Figure 4.26: Time-frequency spectrogram of aLIGO L1 raw strain data near GW170817.

4. ANALYSIS AND CALCULATION OF THEORETICAL WAVEFORM

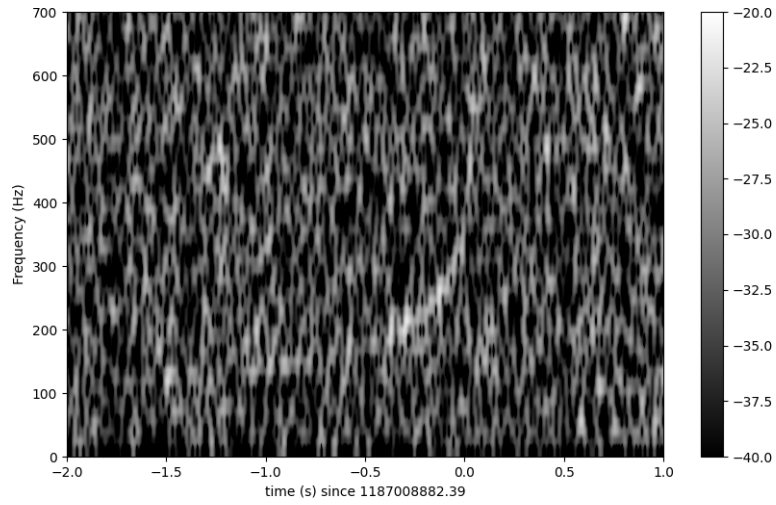


Figure 4.27: Time-frequency spectrogram of aLIGO H1 whitened strain data near GW170817.

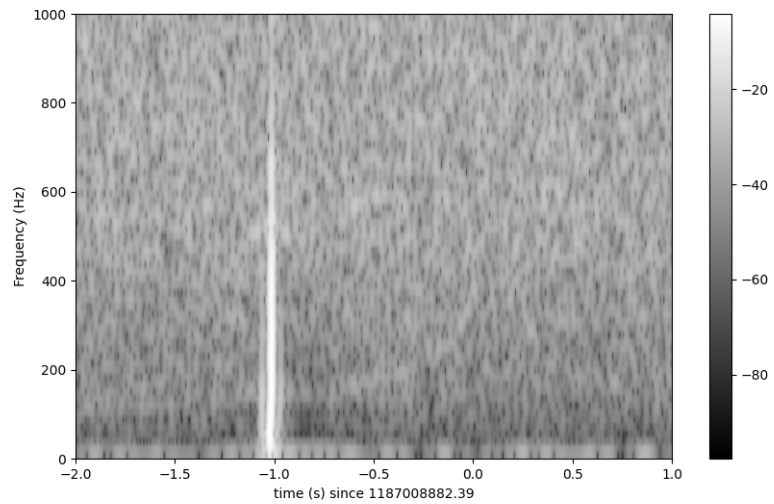


Figure 4.28: Time-frequency spectrogram of aLIGO L1 whitened strain data near GW170817.

As expected (based on our whitened data in figure 4.21), the L1 detector has striking vertical flash thanks to the simultaneous gamma-ray beam mainly detected on the L1 detector. On the other hand, the H1

4. ANALYSIS AND CALCULATION OF THEORETICAL WAVEFORM

has a beautiful wide chirp going on that can be seen on both raw and whitened data spectrograms. It is wider because we chose a smaller interval, if we chose a larger interval it would look more like chirps for the two events analyzed before (subsections 4.1.3 and 4.2.3).

5 Conclusions

Our goal within this thesis was to analyze three of the most known gravitational wave detections and couple them with a calculated theoretical waveform that would fit measured data obtained from GWOSC.

In the first chapter, we showed how they look while warping the spacetime and where they come from. We explained that they can come from not only a collapsing system but also from non-perfectly spherical neutron stars. We continued with the chapter by explaining how to detect gravitational waves. We introduced some history of gravitational wave detectors following up with a small interferometry lecture that is used in the detectors. Lastly, we listed one of the most important gravitational wave detectors that are functioning and detecting at this moment with some that will soon be built.

The second chapter presents the basis of The General Theory of Relativity. We dived into the history of the origin, and later to the "founding block", the Einstein field equation. We discussed the equation and explained every part of it.

The third chapter is the start of our analysis. We introduced reasons and tools for analysis and we dipped toes to some of the parameters that will be needed for the analysis.

In the last fourth chapter, the fun begins. We started analyzing the obtained data from GWOSC. As goes for GW150914 and GW170814 with the measured data from GWOSC, everything went well but the theoretical waveform was quite the bumpy ride. We found out that we needed to correct the values of masses used in calculations ($m_{1,2}$) for the theoretical waveform to fit and couple nicely the measured data. The problem is that the correction was not the same at both events meaning we cannot say it is a statistical error. The corrections were also big fractions of the masses themselves (ranging from 15% to 20% of the used masses). With the help of published papers on studied events, we were able to find out that the models are hard to determine because of the uncertainties and basically the scientists have their own special methods to do this [14] [33] [34]. If we would compare our two-formula approach to calculate the waveform and their special methods, we would find out that maybe therein lies the rub. When it comes to GW170817, the only thing testing the information of the data

5. CONCLUSIONS

are the spectrometers. On the other hand, while doing research for this thesis, we found out that the chirp function made from the measured data of this event is nowhere to be found. Even in the paper about this event, there is only one figure that could be compared to our measured data and that is the raw LIGO-Livingston data that were cleaned differently than we did in our analysis with added glitch model ([34] figure 2). By that, we can predict that the data itself is not the best for the analysis we are doing.

References

1. *Philosophy and science. PDF | Notes to Philosophy 167: Class 13 – Newton's De Motu Corporum in Gyrum (i.e. Version 1) – Complete.* Smith, George Erwin. Available also from: <http://hdl.handle.net/10427/012921>.
2. EINSTEIN, Albert. *Relativity: The special and general theory.* 1st ed. Henry Holt and Company, 1920.
3. LIGO. *All About Gravitational Waves* [online]. [visited on 2023-11-18]. Available from: <https://www.ligo.caltech.edu/page/gravitational-waves>.
4. LIGO. *Sources and Types of Gravitational Waves* [online]. [visited on 2024-05-08]. Available from: <https://www.ligo.caltech.edu/page/gw-sources>.
5. WEBER, J. Evidence for Discovery of Gravitational Radiation. *Phys. Rev. Lett.* 1969, vol. 22, pp. 1320–1324. Available from doi: 10.1103/PhysRevLett.22.1320.
6. GRAVITATIONAL PHYSICS (ALBERT EINSTEIN INSTITUTE), Max Planck Institute for. *Prof. Dr. Heinz Billing dies on 4 January 2017 at the age of 102* [online]. [visited on 2024-05-08]. Available from: <https://www.aei.mpg.de/192485/obituary-heinz-billing>.
7. JANÍK, Jan. *Astronomické pozorování.* 1.1. vyd. Ústav teoretické fyziky a astrofyziky, Přírodovědecká fakulta Masarykovy univerzity, 2021.
8. MICHELSON, A. A.; MORLEY, E. W. On the relative motion of the Earth and the luminiferous ether. *American Journal of Science.* 1887, vol. s3-34, no. 203, pp. 333–345. Available from doi: 10.2475/ajs.s3-34.203.333.
9. GEO600. *What is GEO600?* [online]. [visited on 2024-02-21]. Available from: <https://www.geo600.org/23386/what-is-geo600>.
10. LIGO. *About the LSC* [online]. [visited on 2024-02-21]. Available from: <https://www.ligo.org/about.php>.

REFERENCES

11. E.V, Laser Zentrum Hannover. *Light for innovation: profile of the LZH* [online]. [visited on 2024-02-21]. Available from: <https://www.lzh.de/en/about-us/profile>.
12. LIGO. *About* [online]. [visited on 2024-02-21]. Available from: <https://www.ligo.caltech.edu/page/about>.
13. LIGO. *LIGO-India: A Planned Joint India-US Detector* [online]. [visited on 2024-05-08]. Available from: <https://www.ligo.caltech.edu/page/ligo-india>.
14. ABBOTT, B. P. et al. Observation of Gravitational Waves from a Binary Black Hole Merger. *Phys. Rev. Lett.* 2016, vol. 116, p. 061102. Available from DOI: 10.1103/PhysRevLett.116.061102.
15. VIRGO. *Virgo History* [online]. [visited on 2024-02-25]. Available from: <https://www.virgo-gw.eu/about/virgo-history/>.
16. VIRGO. *EGO* [online]. [visited on 2024-02-25]. Available from: <https://www.virgo-gw.eu/about/ego/>.
17. AKUTSU, T et al. Overview of KAGRA: Detector design and construction history. *Progress of Theoretical and Experimental Physics.* 2020, vol. 2021, no. 5, 05A101. ISSN 2050-3911. Available from DOI: 10.1093/ptep/ptaa125.
18. *LIGO, Virgo and KAGRA Observing run plans* [online]. LIGO-Virgo-KAGRA (LVK) Collaboration [visited on 2024-02-25]. Available from: <https://observing.docs.ligo.org/plan/>.
19. ALBERTINI, Angelica. *Einstein Telescope: a 3rd-generation gravitational-wave detector* [Presented on GWCZ workshop]. 2023.
20. *Introduction* [online]. Einstein Telescope [visited on 2024-02-25]. Available from: <https://www.et-gw.eu/>.
21. BABAK, Stanislav. *Search for Gravitational Waves at Low Frequencies* [Presented on GWCZ workshop]. 2023.
22. *LISA, Laser Interferometer Space Antena* [online]. NASA [visited on 2024-02-25]. Available from: <https://lisa.nasa.gov/>.
23. TINTO, Massimo; DHURANDHAR, Sanjeev V. Time-Delay Interferometry. *Living Reviews in Relativity.* 2005, vol. 8, no. 1. ISSN 1433-8351. Available from DOI: 10.12942/lrr-2005-4.

REFERENCES

24. GIMBEL, Steven. *Einstein & His General Theory of Relativity* [online]. [visited on 2023-10-07]. Available from: <https://yalebooks.yale.edu/2015/04/29/einstein-his-general-theory-of-relativity/>.
25. M. P. HOBSON G. P. EFSTATHIOU, A. N. LASENBY. *General Relativity - An Introduction for Physicists*. Cambridge University Press, 2006.
26. HIRVONEN, Ville. *The Ricci Tensor: A Complete Guide With Examples*. Available also from: <https://profoundphysics.com/the-ricci-tensor/>.
27. *Why Detect Them?* [online]. LIGO [visited on 2024-02-27]. Available from: <https://www.ligo.caltech.edu/page/why-detect-gw>.
28. MAGGIORE, Michele. *Gravitational Waves: Volume 1: Theory and Experiments*. Oxford University Press, 2008.
29. ABBOTT, Rich et al. Open data from the first and second observing runs of Advanced LIGO and Advanced Virgo. *SoftwareX*. 2021, vol. 13, p. 100658. Available from doi: 10.1016/j.softx.2021.100658.
30. VIRTANEN, Pauli; GOMMERS, Ralf; OLIPHANT, Travis E.; HABERLAND, Matt; REDDY, Tyler; COURNAPEAU, David; BUROVSKI, Evgeni; PETERSON, Pearu; WECKESSER, Warren; BRIGHT, Jonathan; VAN DER WALT, Stéfan J.; BRETT, Matthew; WILSON, Joshua; MILLMAN, K. Jarrod; MAYOROV, Nikolay; NELSON, Andrew R. J.; JONES, Eric; KERN, Robert; LARSON, Eric; CAREY, C J; POLAT, İlhan; FENG, Yu; MOORE, Eric W.; VANDERPLAS, Jake; LAXALDE, Denis; PERKTOLD, Josef; CIMRMAN, Robert; HENRIKSEN, Ian; QUINTERO, E. A.; HARRIS, Charles R.; ARCHIBALD, Anne M.; RIBEIRO, Antônio H.; PEDREGOSA, Fabian; VAN MULBREGT, Paul; SCIPY 1.0 CONTRIBUTORS. SciPy 1.0: Fundamental Algorithms for Scientific Computing in Python. *Nature Methods*. 2020, vol. 17, pp. 261–272. Available from doi: 10.1038/s41592-019-0686-2.
31. *SIGNAL PROCESSING WITH GW150914 OPEN DATA* [online]. GWOSC [visited on 2024-03-27]. Available from: https://gwosc.org/GW150914data/GW150914_tutorial.html.

REFERENCES

32. *BINARY BLACK HOLE SIGNALS IN LIGO OPEN DATA* [online]. GWOSC [visited on 2024-03-27]. Available from: https://github.com/gwosc-tutorial/LOSC_Event_tutorial/blob/master/LOSC_Event_tutorial.ipynb.
33. ABBOTT, B. P. et al. GW170814: A Three-Detector Observation of Gravitational Waves from a Binary Black Hole Coalescence. *Physical Review Letters*. 2017, vol. 119, no. 14. ISSN 1079-7114. Available from DOI: 10.1103/physrevlett.119.141101.
34. ABBOTT, B. P. et al. GW170817: Observation of Gravitational Waves from a Binary Neutron Star Inspiral. *Physical Review Letters*. 2017, vol. 119, no. 16. ISSN 1079-7114. Available from DOI: 10.1103/physrevlett.119.161101.

Index

A

Advanced Virgo, 11
AE, 15
aLIGO, 10
ASD, 34

B

Bandpassing, 35
BNS, 5
BS, 23
Burst GWs, 6

C

c, 18
Chirp, 43
Compact Binary Inspiral GWs, 5
Constructive interference, 7
Continuous GWs, 5
Cosmological constant, 18

D

Destructive interference, 7

E

EFE, 15
EGO, 11
Einstein's tensor, 16
EMRIs, 13
Energy-momentum tensor, 19
ER, 21
ET, 12

F

FFT, 34

G

G, 18

GEO600, 10

GTR, 6

GW150914, 21

GW170814, 21

GW170817, 21

GWs, 3

I

Initial LIGO, 10

K

KAGRA, 12

L

LIGO, 10

LIGO-India, 10

LISA, 12

LSC, 11

LVC, 11

M

Michelson interferometer, 8

N

Nyquist frequency, 34

O

O1, 12

O2, 12

O3, 12

O4, 12

P

PSD, 34

R

Ricci curvature tensor, 16

Ricci scalar, 17

INDEX

S

Stochastic GWs, 6

STR, 15

T

TW, 35

V

Virgo, 11

A Appendix

A.1 Codes with steps for GW150914

As mentioned in the main text we will be using code provided by GWOSC from their listed tutorials with some changes.[31][32]

A.1.1 Packages

Step 1 - Importing packages We wrote all the calculations and plotted the data in Python programming language so for us to be able to start it is important to import packages that we will use in making theoretical waveforms as well as in processing measured data from GWOSC.

```
1 import numpy as np
2 from scipy import signal
3 from scipy.interpolate import interp1d
4 from scipy.signal import butter, filtfilt,
   iirdesign, zpk2tf, freqz
5
6
7 %matplotlib inline
8 %config InlineBackend.figure_format = 'retina'
9 import matplotlib.pyplot as plt
10 import matplotlib.mlab as mlab
11 import h5py
12
13
14 import readligo as rl
15
16 import scipy.constants as const
```

Listing A.1: Importing packages

A.1.2 Measured data

Step 2 - Importing data and defining factors We used data downloaded from GWOSC as mentioned in subsection 3.2.2

```
1 #H1
2 fn_H1 = 'H-H1_GWOSC_4KHZ_R1-1126259447-32.hdf5'
```

A. APPENDIX

```
3 strain_H1, time_H1, chan_dict_H1 = rl.loaddata(  
    fn_H1, 'H1')  
4  
5 #L1  
6 fn_L1 = 'L-L1_GWOSC_4KHZ_R1-1126259447-32.hdf5'  
7 strain_L1, time_L1, chan_dict_L1 = rl.loaddata(  
    fn_L1, 'L1')  
8  
9 #sampling rate:  
10 fs = 4096  
11  
12 #both H1 and L1 will have the same time vector, so:  
13 time_EV = time_H1  
14  
15 #the time sample interval (uniformly sampled!)  
16 dt = time_EV[1] - time_EV[0]
```

Listing A.2: Importing data and defining factors

Step 3 - Plotting raw data Where we also defined the time of the event that will be used in further codes.

```
1 tevent = 1126259462.4      # GPS time of the event  
2 deltat = 5.                # seconds around the  
    event  
3  
4 # index into the strain time series for this time  
    interval:  
5 indxt = np.where((time_H1 >= tevent-deltat) & (  
    time_H1 < tevent+deltat))  
6  
7 plt.figure()  
8 plt.plot(time_H1[indxt]-tevent, strain_H1[indxt],  
    label='H1 strain', color='c')  
9 plt.plot(time_L1[indxt]-tevent, strain_L1[indxt],  
    label='L1 strain', color='lightpink')  
10 plt.xlabel('time (s) since '+str(tevent))  
11 plt.ylabel('strain')  
12 plt.legend(loc='lower right')
```

Listing A.3: Plotting raw data

Step 4 - Defining FFT/Interpolations of the ASDs These are the first steps to whitening the data.

```

1 #number of sample for the FFT:
2 NFFT = 1*fs
3 fmin = 10
4 fmax = 2000
5 Pxx_H1, freqs = mlab.psd(strain_H1, Fs = fs, NFFT =
    NFFT)
6 Pxx_L1, freqs = mlab.psd(strain_L1, Fs = fs, NFFT =
    NFFT)
7
8 # We will use interpolations of the ASDs computed
    above for whitening:
9 psd_H1 = interp1d(freqs, Pxx_H1)
10 psd_L1 = interp1d(freqs, Pxx_L1)
11
12 # plot the ASDs:
13 plt.figure()
14 plt.loglog(freqs, np.sqrt(Pxx_H1),label='H1 strain',
    , color="c")
15 plt.loglog(freqs, np.sqrt(Pxx_L1),label='L1 strain',
    , color = 'lightpink')
16 plt.axis([fmin, fmax, 1e-24, 1e-19])
17 plt.grid('on')
18 plt.ylabel('ASD (strain/rtHz)')
19 plt.xlabel('Freq (Hz)')
20 plt.legend(loc='upper center')

```

Listing A.4: FFT and ASDs

Step 5 - Function to whiten the data We are transforming data from the Fourier domain back to the frequency domain, deciding it by the ASDs.

```

1 # function to whiten data
2 def whiten(strain, interp_psd, dt):
3     Nt = len(strain)
4     freqs = np.fft.rfftfreq(Nt, dt)
5
6     # whitening: transform to freq domain, divide
    by asd, then transform back,
7     # taking care to get normalization right.
8     hf = np.fft.rfft(strain)
9     white_hf = hf / (np.sqrt(interp_psd(freqs) /dt
    /2.))
10    white_ht = np.fft.irfft(white_hf, n=Nt)
11    return white_ht

```

```

12
13 # now whiten the data from H1 and L1:
14 strain_H1_whiten = whiten(strain_H1,psd_H1,dt)
15 strain_L1_whiten = whiten(strain_L1,psd_L1,dt)

```

Listing A.5: Whitening function and whitening of data

Step 6 - Bandpassing and plotting whitened data Now let us define the interval of frequencies that we will "let through" for the band passing and plot the whitened data.

```

1 # We need to suppress the high frequencies with
  some bandpassing:
2 bb, ab = butter(4, [20.*2./fs, 300.*2./fs], btype='
  band')
3 strain_H1_whitenbp = filtfilt(bb, ab,
  strain_H1_whiten)
4 strain_L1_whitenbp = filtfilt(bb, ab,
  strain_L1_whiten)
5 k=0
6
7 # plot the data after whitening:
8 # first, shift L1 by 7 ms, and invert.
9 strain_L1_shift = -np.roll(strain_L1_whitenbp,int
  (0.007*fs))
10
11 plt.figure()
12 plt.plot(time_EV-tevent-0.0215, strain_H1_whitenbp, '
  c', label='H1 strain')
13 plt.plot(time_EV-tevent-0.0215, strain_L1_shift, '
  lightpink', label='L1 strain')
14
15 plt.xlim([-0.1,0.05])
16 plt.ylim([-4,4])
17 plt.xlabel('time (s) since '+str(tevent))
18 plt.ylabel('whitented strain')
19 plt.legend(loc='lower left')

```

Listing A.6: Bandpassing and final look at the data

A.1.3 Theoretical waveform

Step 1 - Defining parameters Just so we do not need to write the numerical values over and over again.

```

1 N=1000 #numbers of steps used in plotting
2 pc = const.parsec #parsec
3 Mpc = 1.e6*pc #megaparsec
4 pi=const.pi #pi
5 G= const.gravitational_constant #gravitational
  constant
6 c_light= const.speed_of_light #speed of light
7 #choosing of the time of the collision, we chose 0
  because the measured data from GWOSC are
  adjusted so the collision is at time zero
8 t_coal=0.
9 #with t_coal and t_max we are defining time
  interval where we want to calculate our
  theoretical waveform
10 t_max = 0.3
11 m_1=(35.6-3.1-6.5)*1.98840987e+30 #Primary mass
12 m_2=(30.6-4.4-6.5)*1.98840987e+30 #Secondary mass
13 dist=(452.-170)*Mpc #Luminosity distance
14
15 #definition of parameters used for chirp mass
  calculation
16 M_tot=m_1+m_2
17 numerator=m_1*m_2
18 denominator=M_tot
19
20 m_chirp=(numerator**(3./5.))/(denominator**(1./5.))
  #chirp mass
21
22 time_WF = np.linspace(t_coal+t_max/N,t_max, N,
  endpoint = True) #time (inverted)
23 neg_time_WF = -1.*time_WF
  #time interval used as a x values
  for plot

```

Listing A.7: Shortcuts for values

Step 2 - Calculating needed parameters Using the formulas mentioned in subsection ??.

```

1 f=(1./pi)*((c_light**3./((G*m_chirp)))**(5./8.))
  *(5./(256.*(t_coal+time_WF)))**(3./8.) #
  frequency
2
3 h_0=4./dist*(G*m_chirp/c_light/c_light)**(5./3.)*(
  pi*f/c_light)**(2./3.) #amplitude

```

Listing A.8: Calculation of parameters for wave function

Step 3 - Plotting the wave The final step is to pluck the parameters into basic wave formula also mentioned in subsection ??.

```

1 # Plotting
2 waveform = h_0*np.cos(2.*pi*f*time_WF)
3
4 plt.plot(neg_time_WF, waveform, '-', color='dimgrey')
5 plt.xlim(-t_max, t_coal)
6 plt.xlabel('time (s) since 1126259462.4')
7 plt.ylabel('strain')
8 plt.title('Theoretical waveform for data near
           GW150914')
```

Listing A.9: Calculation of parameters for wave function

A.1.4 Combination of MD and TW

```

1 #now plotting whitened data with theoretical waveform
2
3 plt.figure()
4 plt.plot(time_EV-tevent-0.0215, strain_H1_whitenbp, 'c',
           label='H1 strain')
5 plt.plot(time_EV-tevent-0.0215, strain_L1_shift, 'lightpink',
           label='L1 strain')
6 plt.plot(neg_time_WF, (waveform/10e-22), '-', color='dimgrey',
           label='TW')
7
8
9 plt.xlim([-0.1, 0.05])
10 plt.ylim([-4, 4])
11 plt.xlabel('time (s) since '+str(tevent))
12 plt.ylabel('whitented strain')
13 plt.legend(loc='lower left')
```

Listing A.10: Combining MD and TW

A.1.5 Spectrograms

Step 1 - Plotting the raw data We started by defining the time interval, following up with defining the FFS we are going to use, and choosing the colormap so everything can be read. In the end, we plotted it.

```
1 if make_plots:
2     # index into the strain time series for this
3     # time interval:
4     indxt = np.where((time_EV >= tevent-deltat) & (
5     time_EV < tevent+deltat))
6
7     # pick a shorter FFT time interval, like 1/8 of
8     # a second:
9     NFFT = int(fs/8)
10    # and with a lot of overlap, to resolve short-
11    # time features:
12    NOVL = int(NFFT*15./16)
13    # and choose a window that minimizes "spectral
14    # leakage"
15    window = np.blackman(NFFT)
16
17    # the colormap is all-important!
18    spec_cmap='gist_gray'
19
20    # Plot the H1 spectrogram:
21    plt.figure(figsize=(10,6))
22    spec_H1, freqs, bins, im = plt.specgram(
23    strain_H1[indxt], NFFT=NFFT, Fs=fs, window=
24    window,
25
26    noverlap=NOVL, cmap=spec_cmap, xextent=[-deltat,
27    deltat])
28    plt.xlabel('time (s) since '+str(tevent))
29    plt.ylabel('Frequency (Hz)')
30    plt.colorbar()
31    plt.axis([-deltat, deltat, 0, 2000])
32
33    # Plot the L1 spectrogram:
34    plt.figure(figsize=(10,6))
35    spec_L1, freqs, bins, im = plt.specgram(
36    strain_L1[indxt], NFFT=NFFT, Fs=fs, window=
37    window,
38
39    noverlap=NOVL, cmap=spec_cmap, xextent=[-deltat,
40    deltat])
41    plt.xlabel('time (s) since '+str(tevent))
42    plt.ylabel('Frequency (Hz)')
43    plt.colorbar()
```

```
33 plt.axis([-deltat, deltat, 0, 2000])
```

Listing A.11: Making and plotting spectrogram of raw data

Step 3 - Plotting the whitened data Same as step one but using the whitened data.

```
1 if make_plots:
2     # plot the whitened data, zooming in on the
3     # signal region:
4
5     # pick a shorter FFT time interval, like 1/16
6     # of a second:
7     NFFT = int(fs/16.0)
8     # and with a lot of overlap, to resolve short-
9     # time features:
10    NOVL = int(NFFT*15/16.0)
11    # choose a window that minimizes "spectral
12    # leakage"
13    window = np.blackman(NFFT)
14
15    # Plot the H1 whitened spectrogram around the
16    # signal
17    plt.figure(figsize=(10,6))
18    spec_H1, freqs, bins, im = plt.specgram(
19    strain_H1_whiten[indxt], NFFT=NFFT, Fs=fs,
20    window=window,
21
22    noverlap=NOVL, cmap=spec_cmap, xextent=[-deltat,
23    deltat])
24    plt.xlabel('time (s) since '+str(tevent))
25    plt.ylabel('Frequency (Hz)')
26    plt.colorbar()
27    plt.axis([-0.5, 0.5, 0, 500])
28
29    # Plot the L1 whitened spectrogram around the
30    # signal
31    plt.figure(figsize=(10,6))
32    spec_H1, freqs, bins, im = plt.specgram(
33    strain_L1_whiten[indxt], NFFT=NFFT, Fs=fs,
34    window=window,
35
36    noverlap=NOVL, cmap=spec_cmap, xextent=[-deltat,
37    deltat])
```

```

26 plt.xlabel('time (s) since '+str(tevent))
27 plt.ylabel('Frequency (Hz)')
28 plt.colorbar()
29 plt.axis([-0.5, 0.5, 0, 500])

```

Listing A.12: Making and plotting spectrogram of raw data

A.2 Code for GW170814

As goes for this detection and later the GW170817, we will not be including steps for the code. We were following the same steps so it will not be necessary.

```

1 #importing packages
2
3 import numpy as np
4 from scipy import signal
5 from scipy.interpolate import interp1d
6 from scipy.signal import butter, filtfilt, iirdesign,
   zpk2tf, freqz
7
8
9 %matplotlib inline
10 %config InlineBackend.figure_format = 'retina'
11 import matplotlib.pyplot as plt
12 import matplotlib.mlab as mlab
13 import h5py
14
15
16 import readligo as rl
17
18 import scipy.constants as const
19
20 # H1
21 fn_H1 = 'H-H1_GWOSC_4KHZ_R1-1186741846-32.hdf5'
22 strain_H1, time_H1, chan_dict_H1 = rl.loaddata(fn_H1, 'H1
   ')
23
24 # L1
25 fn_L1 = 'L-L1_GWOSC_4KHZ_R1-1186741846-32.hdf5'
26 strain_L1, time_L1, chan_dict_L1 = rl.loaddata(fn_L1, 'L1
   ')
27
28 # sampling rate:

```

A. APPENDIX

```
29 fs = 4096
30
31 # both H1 and L1 will have the same time vector, so:
32 time_EV = time_H1
33
34 # the time sample interval (uniformly sampled!)
35 dt = time_EV[1] - time_EV[0]
36
37 #calculation of our theoretical waveform
38 N=1000
39 pc = const.parsec
40 Mpc = 1.e6*pc
41 pi=const.pi
42 G= const.gravitational_constant
43 c_light= const.speed_of_light
44 t_coal=0.
45 t_max = 0.3
46 m_1=(30.6-3.0-4.6)*1.98840987e+30
47 m_2=(25.2-0.3-4.6)*1.98840987e+30
48 dist=(600-220)*Mpc
49
50 M_tot=m_1+m_2
51 numerator=m_1*m_2
52 denominator=M_tot
53
54 m_chirp=(numerator**(3./5.))/(denominator**(1./5.))
55
56
57 time_WF = np.linspace(t_coal+t_max/N,t_max, N, endpoint =
    True) #time (inverted)
58 neg_time_WF = -1.*time_WF
    #time
59
60 f=(1./pi)*((c_light**3./((G*m_chirp)))**(5./8.))
    *(5./(256.*(t_coal+time_WF))**(3./8.)) #frequency
61
62 h_0=4./dist*(G*m_chirp/c_light/c_light)**(5./3.)*(pi*f/
    c_light)**(2./3.) #amplitude
63
64 waveform = h_0*np.cos(2.*pi*f*time_WF)
65
66
67
68 # Plotting
69 plt.plot(neg_time_WF, waveform, '--', color='dimgrey')
```

```

70 plt.xlim(-t_max,t_coal)
71 plt.xlabel('time (s) since 1126259462.4')
72 plt.ylabel('strain')
73
74 # Show the plot
75 plt.show()
76
77 # plot raw +- 3 seconds around the event:
78 tevent = 1186741861.5
79 deltat = 3.
80
81 # index into the strain time series for this time
    interval:
82 indxt = np.where((time_H1 >= tevent-deltat) & (time_H1 <
    tevent+deltat))
83
84 plt.figure()
85 plt.plot(time_H1[indxt]-tevent, strain_H1[indxt], label='H1
    strain', color='c')
86 plt.plot(time_L1[indxt]-tevent, strain_L1[indxt], label='L1
    strain', color='lightpink')
87 plt.xlabel('time (s) since '+str(tevent))
88 plt.ylabel('strain')
89 plt.legend(loc='lower right')
90
91 # number of sample for the fast fourier transform:
92 NFFT = 1*fs
93 fmin = 10
94 fmax = 2000
95 Pxx_H1, freqs = mlab.psd(strain_H1, Fs = fs, NFFT = NFFT)
96 Pxx_L1, freqs = mlab.psd(strain_L1, Fs = fs, NFFT = NFFT)
97
98 # We will use interpolations of the ASDs computed above
    for whitening:
99 psd_H1 = interp1d(freqs, Pxx_H1)
100 psd_L1 = interp1d(freqs, Pxx_L1)
101
102 # plot the ASDs:
103 plt.figure()
104 plt.loglog(freqs, np.sqrt(Pxx_H1), label='H1 strain',
    color="c")
105 plt.loglog(freqs, np.sqrt(Pxx_L1), label='L1 strain',
    color='lightpink')
106 plt.axis([fmin, fmax, 1e-24, 1e-19])
107 plt.grid('on')

```

A. APPENDIX

```
108 plt.ylabel('ASD (strain/rtHz)')
109 plt.xlabel('Freq (Hz)')
110 plt.legend(loc='upper center')
111
112
113 # function to whiten data
114 def whiten(strain, interp_psd, dt):
115     Nt = len(strain)
116     freqs = np.fft.rfftfreq(Nt, dt)
117
118     # whitening: transform to freq domain, divide by asd,
119     # then transform back,
120     # taking care to get normalization right.
121     hf = np.fft.rfft(strain)
122     white_hf = hf / (np.sqrt(interp_psd(freqs) / dt / 2.))
123     white_ht = np.fft.irfft(white_hf, n=Nt)
124     return white_ht
125
126 # now whiten the data from H1 and L1, and also the NR
127 # template:
128 strain_H1_whiten = whiten(strain_H1, psd_H1, dt)
129 strain_L1_whiten = whiten(strain_L1, psd_L1, dt)
130
131 # function to whiten data
132 def whiten(strain, interp_psd, dt):
133     Nt = len(strain)
134     freqs = np.fft.rfftfreq(Nt, dt)
135
136     # whitening: transform to freq domain, divide by asd,
137     # then transform back,
138     # taking care to get normalization right.
139     hf = np.fft.rfft(strain)
140     white_hf = hf / (np.sqrt(interp_psd(freqs) / dt / 2.))
141     white_ht = np.fft.irfft(white_hf, n=Nt)
142     return white_ht
143
144 # now whiten the data from H1 and L1, and also the NR
145 # template:
146 strain_H1_whiten = whiten(strain_H1, psd_H1, dt)
147 strain_L1_whiten = whiten(strain_L1, psd_L1, dt)
148
149 # We need to suppress the high frequencies with some
150 # bandpassing:
151 bb, ab = butter(4, [20.*2./fs, 300.*2./fs], btype='band')
152 strain_H1_whitenbp = filtfilt(bb, ab, strain_H1_whiten)
```

```
148 strain_L1_whitenbp = filtfilt(bb, ab, strain_L1_whiten)
149 k=0
150
151 # plot the data after whitening:
152 # first, shift L1 by 7 ms, and invert. See the GW150914
    detection paper for why!
153 strain_L1_shift = -np.roll(strain_L1_whitenbp, int(0.007*
    fs))
154
155 plt.figure()
156 plt.plot(time_EV-tevent-0.0215, strain_H1_whitenbp, 'c',
    label='H1 strain')
157 plt.plot(time_EV-tevent-0.0215, strain_L1_shift, 'lightpink',
    label='L1 strain')
158
159 plt.xlim([-0.1, 0.05])
160 plt.ylim([-4, 4])
161 plt.xlabel('time (s) since '+str(tevent))
162 plt.ylabel('whitented strain')
163 plt.legend(loc='lower left')
164
165 #now plotting whitend data with theoretical waveform
166
167 plt.figure()
168 plt.plot(time_EV-tevent-0.024, strain_H1_whitenbp, 'c',
    label='H1 strain')
169 plt.plot(time_EV-tevent-0.024, strain_L1_shift, 'lightpink',
    label='L1 strain')
170 plt.plot(neg_time_WF, (waveform/10e-22), '-', color='
    dimgrey', label='TW')
171
172
173 plt.xlim([-0.1, 0.05])
174 plt.ylim([-4, 4])
175 plt.xlabel('time (s) since '+str(tevent))
176 plt.ylabel('whitented strain')
177 plt.legend(loc='lower left')
178
179 #spectograms
180 make_plots = 1
181 eventname = 'GW170814'
182 plottype = "png"
183
184 if make_plots:
```

A. APPENDIX

```
185     # index into the strain time series for this time
186     interval:
187     indxt = np.where((time_EV >= tevent-deltat) & (
188     time_EV < tevent+deltat))
189
190     # pick a shorter FFT time interval, like 1/8 of a
191     second:
192     NFFT = int(fs/8)
193     # and with a lot of overlap, to resolve short-time
194     features:
195     NOVL = int(NFFT*15./16)
196     # and choose a window that minimizes "spectral
197     leakage"
198     window = np.blackman(NFFT)
199
200     spec_cmap='gist_gray'
201
202     # Plot the H1 spectrogram:
203     plt.figure(figsize=(10,6))
204     spec_H1, freqs, bins, im = plt.specgram(strain_H1[
205     indxt], NFFT=NFFT, Fs=fs, window=window,
206     noverlap=NOVL
207     , cmap=spec_cmap, xextent=[-deltat,deltat])
208     plt.xlabel('time (s) since '+str(tevent))
209     plt.ylabel('Frequency (Hz)')
210     plt.colorbar()
211     plt.axis([-deltat, deltat, 0, 2000])
212
213     # Plot the L1 spectrogram:
214     plt.figure(figsize=(10,6))
215     spec_H1, freqs, bins, im = plt.specgram(strain_L1[
216     indxt], NFFT=NFFT, Fs=fs, window=window,
217     noverlap=NOVL
218     , cmap=spec_cmap, xextent=[-deltat,deltat])
219     plt.xlabel('time (s) since '+str(tevent))
220     plt.ylabel('Frequency (Hz)')
221     plt.colorbar()
222     plt.axis([-deltat, deltat, 0, 2000])
223
224     if make_plots:
225         # plot the whitened data, zooming in on the signal
226         region:
227
228         # pick a shorter FFT time interval, like 1/16 of a
229         second:
```

```
219     NFFT = int(fs/16.0)
220     # and with a lot of overlap, to resolve short-time
features:
221     NOVL = int(NFFT*15/16.0)
222     # choose a window that minimizes "spectral leakage"
223     window = np.blackman(NFFT)
224
225     # Plot the H1 whitened spectrogram around the signal
226     plt.figure(figsize=(10,6))
227     spec_H1, freqs, bins, im = plt.specgram(
strain_H1_whiten[indxt], NFFT=NFFT, Fs=fs, window=
window,
228                                     noverlap=NOVL
, cmap=spec_cmap, xextent=[-deltat,deltat])
229     plt.xlabel('time (s) since '+str(tevent))
230     plt.ylabel('Frequency (Hz)')
231     plt.colorbar()
232     plt.axis([-1, 1, 0, 1000])
233
234
235
236     # Plot the L1 whitened spectrogram around the signal
237     plt.figure(figsize=(10,6))
238     spec_H1, freqs, bins, im = plt.specgram(
strain_L1_whiten[indxt], NFFT=NFFT, Fs=fs, window=
window,
239                                     noverlap=NOVL
, cmap=spec_cmap, xextent=[-deltat,deltat])
240     plt.xlabel('time (s) since '+str(tevent))
241     plt.ylabel('Frequency (Hz)')
242     plt.colorbar()
243     plt.axis([-1, 1, 0, 1000])
```

Listing A.13: Whole code used for analysis of GW170814

A.3 Code for GW170817

```
1 #importing packages
2
3 import numpy as np
4 from scipy import signal
5 from scipy.interpolate import interp1d
6 from scipy.signal import butter, filtfilt, iirdesign,
   zpk2tf, freqz
7
8
9 %matplotlib inline
10 %config InlineBackend.figure_format = 'retina'
11 import matplotlib.pyplot as plt
12 import matplotlib.mlab as mlab
13 import h5py
14
15
16 import readligo as rl
17
18 import scipy.constants as const
19
20 # H1
21 fn_H1 = 'H-H1_GWOSC_4KHZ_R1-1187008867-32.hdf5'
22 strain_H1, time_H1, chan_dict_H1 = rl.loaddata(fn_H1, 'H1
   ')
23
24 # L1
25 fn_L1 = 'L-L1_GWOSC_4KHZ_R1-1187008867-32.hdf5'
26 strain_L1, time_L1, chan_dict_L1 = rl.loaddata(fn_L1, 'L1
   ')
27
28 # sampling rate:
29 fs = 4096
30
31 # both H1 and L1 will have the same time vector, so:
32 time_EV = time_H1
33
34 # the time sample interval (uniformly sampled!)
35 dt = time_EV[1] - time_EV[0]
36
37 #calculation of our theoretical waveform
38 N=1000
39 pc = const.parsec
40 Mpc = 1.e6*pc
```

```

41 pi=const.pi
42 G= const.gravitational_constant
43 c_light= const.speed_of_light
44 t_max = 0.1
45 m_1=1.46*2.*1.e30
46 m_2=1.27*2.*1.e30
47 numerator=m_1*m_2
48 M_tot=m_1+m_2
49
50 denominator=M_tot
51
52 m_chirp=(numerator**(3./5.))/(denominator**(1./5.))
53
54
55 time_WF = np.linspace(t_coal+t_max/N,t_max, N, endpoint =
    True) #time (inverted)
56 neg_time_WF = -1.*time_WF
    #time
57
58 f=(1./pi)*((c_light**3./((G*m_chirp)))**(5./8.))
    *(5./(256.*(t_coal+time_WF))**(3./8.)) #frequency
59
60 h_0=4./dist*(G*m_chirp/c_light/c_light)**(5./3.)*(pi*f/
    c_light)**(2./3.) #amplitude
61
62 waveform = h_0*np.cos(2*pi*f*time_WF)
63
64 plt.plot(neg_time_WF, waveform, '- ', color='dimgrey')
65 plt.xlim(-t_max, t_coal)
66
67 # Show the plot
68 plt.show()
69
70 tevent = 1187008882.39
71 deltat = 2.
72
73 indxt = np.where((time_H1 >= tevent-deltat) & (time_H1 <
    tevent+deltat))
74
75 plt.figure()
76 plt.plot(time_H1[indxt]-tevent, strain_H1[indxt], 'c', label
    ='H1 strain')
77 plt.plot(time_L1[indxt]-tevent, strain_L1[indxt], '
    lightpink', label='L1 strain')
78

```

A. APPENDIX

```
79 plt.xlabel('time (s) since '+str(tevent))
80 plt.ylabel('strain')
81 plt.legend(loc='lower right')
82
83 NFFT = 1*fs
84 fmin = 10
85 fmax = 2000
86 Pxx_H1, freqs = mlab.psd(strain_H1, Fs = fs, NFFT = NFFT)
87 Pxx_L1, freqs = mlab.psd(strain_L1, Fs = fs, NFFT = NFFT)
88
89
90
91 psd_H1 = interp1d(freqs, Pxx_H1)
92 psd_L1 = interp1d(freqs, Pxx_L1)
93
94
95
96 plt.figure()
97 plt.loglog(freqs, np.sqrt(Pxx_H1), 'c', label='H1 strain')
98 plt.loglog(freqs, np.sqrt(Pxx_L1), 'lightpink', label='L1
    strain')
99
100 plt.axis([fmin, fmax, 1e-24, 1e-19])
101 plt.grid('on')
102 plt.ylabel('ASD (strain/rtHz)')
103 plt.xlabel('Freq (Hz)')
104 plt.legend(loc='upper center')
105
106 # function to whiten data
107 def whiten(strain, interp_psd, dt):
108     Nt = len(strain)
109     freqs = np.fft.rfftfreq(Nt, dt)
110
111     # whitening: transform to freq domain, divide by asd,
    then transform back,
112     # taking care to get normalization right.
113     hf = np.fft.rfft(strain)
114     white_hf = hf / (np.sqrt(interp_psd(freqs) /dt/2.))
115     white_ht = np.fft.irfft(white_hf, n=Nt)
116     return white_ht
117
118 # now whiten the data from H1 and L1, and also the NR
    template:
119 strain_H1_whiten = whiten(strain_H1, psd_H1, dt)
120 strain_L1_whiten = whiten(strain_L1, psd_L1, dt)
```

```
121
122 # We need to suppress the high frequencies with some
    bandpassing:
123 bb, ab = butter(4, [30.*2./fs, 200.*2./fs], btype='band')
124 strain_H1_whitenbp = filtfilt(bb, ab, strain_H1_whiten)
125 strain_L1_whitenbp = filtfilt(bb, ab, strain_L1_whiten)
126
127
128
129 # plot the data after whitening:
130 # first, shift L1 by 7 ms, and invert. See the GW150914
    detection paper for why!
131 strain_L1_shift = -np.roll(strain_L1_whitenbp, int(0.007*
    fs))
132
133 plt.figure()
134 plt.plot(time_EV-tevent, strain_H1_whitenbp, 'c', label='H1
    strain')
135 plt.plot(time_EV-tevent, strain_L1_whitenbp, 'lightpink',
    label='L1 strain')
136
137 plt.xlim([-1.1, -0.95])
138 plt.ylim([-30, 30])
139 plt.xlabel('time (s) since '+str(tevent))
140 plt.ylabel('whitented strain')
141 plt.legend(loc='lower left')
142
143
144 #now plotting with Waveform
145
146 plt.figure()
147 plt.plot(time_EV-tevent, strain_H1_whitenbp, 'c', label='H1
    strain')
148 plt.plot(time_EV-tevent, strain_L1_whitenbp, 'lightpink',
    label='L1 strain')
149
150 plt.plot(neg_time_WF-1.0017, (waveform/(10e-23)), '-',
    color='dimgrey', label='TW')
151
152 #1.0017
153 #0.992
154 plt.xlim([-1.10, -0.95])
155 plt.ylim([-30, 30])
156 plt.xlabel('time (s) since '+str(tevent))
157 plt.ylabel('whitented strain')
```

A. APPENDIX

```
158 plt.legend(loc='lower left')
159
160 make_plots = 1
161 eventname = 'GW170817'
162 plottype = "png"
163
164 if make_plots:
165     # index into the strain time series for this time
166     # interval:
167     indxt = np.where((time_EV >= tevent-deltat) & (
168     time_EV < tevent+deltat))
169
170     # pick a shorter FFT time interval, like 1/8 of a
171     # second:
172     NFFT = int(fs/8)
173     # and with a lot of overlap, to resolve short-time
174     # features:
175     NOVL = int(NFFT*15./16)
176     # and choose a window that minimizes "spectral
177     # leakage"
178     # (https://en.wikipedia.org/wiki/Spectral\_leakage)
179     window = np.blackman(NFFT)
180
181     spec_cmap='gist_gray'
182
183     # Plot the H1 spectrogram:
184     plt.figure(figsize=(10,6))
185     spec_H1, freqs, bins, im = plt.specgram(strain_H1[
186     indxt], NFFT=NFFT, Fs=fs, window=window,
187     noverlap=NOVL
188     , cmap=spec_cmap, xextent=[-deltat,deltat])
189     plt.xlabel('time (s) since '+str(tevent))
190     plt.ylabel('Frequency (Hz)')
191     plt.colorbar()
192     plt.axis([-deltat, deltat, 0, 2000])
193
194     # Plot the L1 spectrogram:
195     plt.figure(figsize=(10,6))
196     spec_H1, freqs, bins, im = plt.specgram(strain_L1[
197     indxt], NFFT=NFFT, Fs=fs, window=window,
198     noverlap=NOVL
199     , cmap=spec_cmap, xextent=[-deltat,deltat])
200     plt.xlabel('time (s) since '+str(tevent))
201     plt.ylabel('Frequency (Hz)')
```

```
194 plt.colorbar()
195 plt.axis([-deltat, deltat, 0, 2000])
196
197 if make_plots:
198     # plot the whitened data, zooming in on the signal
199     # region:
200
201     # pick a shorter FFT time interval, like 1/16 of a
202     # second:
203     NFFT = int(fs/16.0)
204     # and with a lot of overlap, to resolve short-time
205     # features:
206     NOVL = int(NFFT*15/16.0)
207     # choose a window that minimizes "spectral leakage"
208     # (https://en.wikipedia.org/wiki/Spectral_leakage)
209     window = np.blackman(NFFT)
210
211     # Plot the H1 whitened spectrogram around the signal
212     plt.figure(figsize=(10,6))
213     spec_H1, freqs, bins, im = plt.specgram(
214     strain_H1_whiten[indxt], NFFT=NFFT, Fs=fs, window=
215     window,
216
217     noverlap=NOVL
218     , cmap=spec_cmap, xextent=[-deltat,deltat], vmin=-40,
219     vmax=-20)
220     plt.xlabel('time (s) since '+str(tevent))
221     plt.ylabel('Frequency (Hz)')
222     plt.colorbar()
223     plt.axis([-2, 1, 0, 700])
224
225     # Plot the L1 whitened spectrogram around the signal
226     plt.figure(figsize=(10,6))
227     spec_H1, freqs, bins, im = plt.specgram(
228     strain_L1_whiten[indxt], NFFT=NFFT, Fs=fs, window=
229     window,
230
231     noverlap=NOVL
232     , cmap=spec_cmap, xextent=[-deltat,deltat])
233     plt.xlabel('time (s) since '+str(tevent))
234     plt.ylabel('Frequency (Hz)')
235     plt.colorbar()
236     plt.axis([-2, 1, 0, 1000])
```

Listing A.14: Whole code used for analysis of GW170817